Paleoceanography and Paleoclimatology

RESEARCH ARTICLE
10.1029/2018PA003478

A Seasonal Model of Nitrogen Isotopes in the Ice Age Antarctic Zone: Support for Weakening of the Southern Ocean Upper Overturning Cell

P. C. Kemeny[1,2], E. R. Kast[1], M. P. Hain[3], S. E. Fawcett[4], F. Fripiat[5], A. S. Studer[5], A. Martínez-García[5], G. H. Haug[5,6], and D. M. Sigman[1]

[1]Department of Geosciences, Princeton University, Princeton, NJ, USA, [2]Division of Geological and Planetary Sciences, California Institute of Technology, Pasadena, CA, USA, [3]Department of Earth and Planetary Sciences, University of California Santa Cruz, Santa Cruz, CA, USA, [4]Department of Oceanography, University of Cape Town, Rondebosch, South Africa, [5]Climate Geochemistry Department, Max Planck Institute for Chemistry, Mainz, Germany, [6]Department of Earth Sciences, ETH Zürich, Zürich, Switzerland

Key Points:
- A two-layer model of Antarctic Zone seasonality that includes upper ocean N cycling captures key N isotopic patterns
- The model indicates that an ice age rise of ~3‰-4‰ in diatom-bound $\delta^{15}N$ requires a >80% reduction in gross NO_3^- supply from deep waters
- This large change implies a weakening of the upper cell of global ocean overturning that passes through the Antarctic surface

Supporting Information:
- Supporting Information S1
- Data Set S1

Correspondence to:
P. C. Kemeny,
pkemeny@caltech.edu

Citation:
Kemeny, P. C., Kast, E. R., Hain, M. P., Fawcett, S. E., Fripiat, F., Studer, A. S., et al. (2018). A seasonal model of nitrogen isotopes in the ice age Antarctic Zone: Support for weakening of the Southern Ocean upper overturning cell. *Paleoceanography and Paleoclimatology*, *33*, 1453–1471. https://doi.org/10.1029/2018PA003478

Received 17 SEP 2018
Accepted 26 NOV 2018
Accepted article online 30 NOV 2018
Published online 21 DEC 2018

Abstract In the Antarctic Zone of the Southern Ocean, the coupled observations of elevated diatom-bound $^{15}N/^{14}N$ ($\delta^{15}N_{db}$) and reduced export production during the ice ages indicates more complete nitrate (NO_3^-) consumption. This evidence points to an ice age decline in gross NO_3^- supply from the deep ocean to the surface wind-mixed layer, which may help to explain the reduced CO_2 levels of the ice age atmosphere. We use a seasonally resolved, two-layer model of the N isotopes in the Antarctic Zone upper ocean to quantify the ice age decline in gross NO_3^- supply implied by the data. When model parameters are varied to reflect reduced gross NO_3^- supply, the concentration of wintertime upper ocean NO_3^- is lowered, but with a much weaker increase in NO_3^- $\delta^{15}N$ than predicted by analytical models such as the Rayleigh and steady state models. Physical mixing is the dominant cause, with a modest contribution from foodweb dynamics. As a result, the observed $\delta^{15}N_{db}$ rise of ~3‰–4‰ must be explained mostly by a greater summertime increase in NO_3^- $\delta^{15}N$ during the ice ages. The high degree of NO_3^- consumption required to generate this summertime $\delta^{15}N$ rise indicates a >80% reduction in gross NO_3^- supply. Half or more of the modern gross NO_3^- supply is from wind-forced Antarctic upwelling that drives the upper cell of Southern Ocean overturning. Thus, the decrease in NO_3^- supply cannot be achieved solely by a decline in vertical mixing or wintertime convection; rather, it requires an ice age weakening of the upper cell.

1. Introduction

The Southern Ocean surface is characterized by rapid supply of nitrate (NO_3^-) and phosphate (PO_4^{3-}) from the underlying deep ocean, such that iron (Fe) and light appear to limit the growth of phytoplankton (Martin, 1990; Sunda & Huntsman, 1997). Incomplete NO_3^- consumption in the Southern Ocean surface and subsequent transport of NO_3^--rich water into the ocean interior increases the fraction of unused (preformed) NO_3^-, which is necessarily accompanied by the degassing of biologically sequestered carbon dioxide (CO_2) back to the atmosphere (Ito & Follows, 2005; Sarmiento & Toggweiler, 1984; Sigman et al., 2010). An increase in Southern Ocean nutrient consumption can enhance the efficiency of the global biological pump and stem the high-latitude CO_2 leak, making it a promising explanation for the lower atmospheric CO_2 concentrations of ice ages (Knox & McElroy, 1984; Sarmiento & Toggweiler, 1984; Siegenthaler & Wenk, 1984).

The Southern Ocean is commonly divided into the polar Antarctic Zone (AZ) and the equatorward Subantarctic Zone (SAZ), with the Polar Frontal Zone (PFZ) between them. Circumpolar Deep Water (CDW) outcrops in the AZ before (1) returning to the deep ocean as Antarctic Bottom Water, (2) forming Antarctic Intermediate Water in the PFZ near the Antarctic Polar Front (APF), or (3) flowing northward into the SAZ. Both the upwelling of deep water and its northward transport constitute parts of the upper cell of Southern Ocean overturning that passes through the AZ surface (Toggweiler et al., 2006), which also includes the subduction of waters in the PFZ and SAZ. The magnitude of upper cell overturning is thought to reflect the residual circulation resulting from the superposition of the wind-driven Ekman upwelling and eddy-associated transport, with the latter largely opposing the former so as to decrease the net rate of upper cell overturning (Marshall & Speer, 2012). Conversely, the lower cell of Southern Ocean overturning reflects the poleward movement of upwelled water and formation of Antarctic Bottom Water. The Southern Antarctic

Circumpolar Current Front is the approximate boundary of poleward and equatorward transport of upwelled water (i.e., the lower and upper cells), dividing the AZ into the southern Polar Antarctic Zone (PAZ) and the northern Open Antarctic Zone (OAZ). There is evidence that both the AZ and SAZ contributed to lower Southern Ocean CO_2 leakage during ice ages, through circulation changes in the AZ (François et al., 1997) and through an Fe-fertilized rise in export production in the SAZ (Martínez-García et al., 2014). Here we focus on the data indicating changes in the AZ.

In sediment cores from the AZ, the glacial intervals are characterized by an elevated $\delta^{15}N$ of the organic matter bound within diatom microfossils ($\delta^{15}N_{db}$, where $\delta^{15}N = (^{15}N/^{14}N)_{sample}/(^{15}N/^{14}N)_{AIR} - 1$ and AIR refers to atmospheric N_2, with values reported in per mil [‰]; Studer et al., 2015, and references therein). These higher values of $\delta^{15}N_{db}$ argue for more complete NO_3^- consumption during ice ages relative to the modern ocean. At the same time, proxies such as thorium-230-normalized fluxes of opal and biogenic barium, as well as the ratio of protactinium to thorium, consistently indicate decreased export production during ice ages (François et al., 1997; Kumar et al., 1993, 1995; Mortlock et al., 1991). The coupled observations of elevated $\delta^{15}N_{db}$ and reduced export production are thought to require a decline in the supply of NO_3^- to the AZ surface (François et al., 1997; Robinson & Sigman, 2008). Other proposals for these coupled observations (Anderson et al., 2002), such as an ice age influence from high-$\delta^{15}N$, sea ice-derived organic matter (Rau et al., 1991), have so far failed to produce a viable alternative explanation (Fripiat et al., 2014).

The ice age reduction in gross nutrient supply, under most circumstances, requires a decline in the rate at which NO_3^--rich CDW is imported into the summertime mixed layer. François et al. (1997) originally referred to the glacial state of reduced nutrient supply as *stratification*, based on the notion that the reduction in vertical communication of waters would involve enhanced density gradients. In an effort to reduce confusion between the observationally inferred reduction in deep/surface exchange and its physical oceanographic cause, we refer to the reduction in exchange itself as ice age *separation*.

A decrease in wind-driven upwelling within the AZ was one of the first physical hypotheses for AZ ice age separation (Sigman & Boyle, 2000; Toggweiler et al., 2006). According to this hypothesis, the colder glacial climate induced an equatorward migration of the Antarctic wind belt, decreasing upwelling in the AZ and thus the strength of the upper cell (Toggweiler et al., 2006). This change may have in turn worked to weaken the lower cell, as follows (De Boer et al., 2008; Toggweiler et al., 2006). A northward shift in the westerly winds would have increased the residence time of water in the AZ surface mixed layer, strengthening salinity-driven density stratification (the halocline) in the AZ upper water column and impeding vertical exchange. This change could have reduced deep ocean ventilation in the AZ, possibly including the abyssal water formation that appears to occur mostly around the Antarctic continent.

These changes, especially the weakening of the lower cell, should have worked to lower atmospheric CO_2. Even in the case of a partially compensating decline in the absolute rates of nutrient assimilation and biological export production, the reduction in gross nutrient supply to the surface ocean could have resulted in elevated fractional nutrient consumption (François et al., 1997; Studer et al., 2015). Both the reduction in abyssal ocean ventilation from the AZ and the increased nutrient consumption would have diminished the high-latitude CO_2 leak to the atmosphere (Hain et al., 2010).

Other physical mechanisms have been proposed for ice age Antarctic separation. A second category of hypotheses involves a decline in abyssal mixing, in effect reducing the demand for new deep water to form around Antarctica (De Boer & Hogg, 2014; Ferrari et al., 2014; Lund et al., 2011; Watson & Naveira Garabato, 2006). The reduced effect of temperature on seawater density at low temperature has been proposed to explain the apparent reduction in Antarctic deep ventilation both at the 2.7 million year intensification of northern hemisphere glaciation (Sigman et al., 2004) and during the late Pleistocene ice ages (De Boer et al., 2007). An expansion of seasonal sea ice during ice ages has been proposed to export brines sufficiently concentrated in salt that they freshened the Antarctic surface and reduced deep water formation (Bouttes et al., 2010). Finally, an expansion of the Antarctic region of buoyancy loss would have increased the residence time of water in the Antarctic surface between ascending from depth and sinking back into the interior, allowing for more complete NO_3^- consumption (Ferrari et al., 2014; Watson et al., 2015).

There is a critical need for additional information with which to test these varied hypotheses. The major impetus for the current study is to provide constraints on the physical changes that may have caused ice

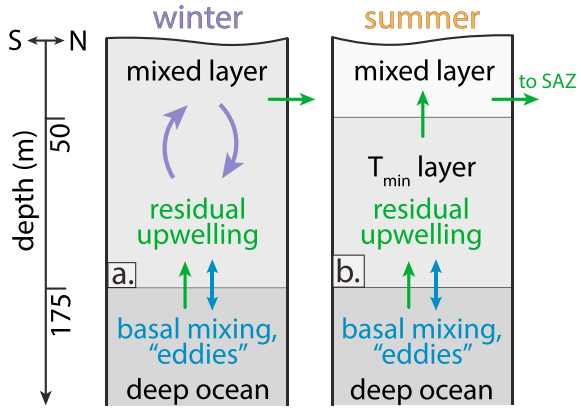

Figure 1. NO_3^- is supplied to the Antarctic Zone upper water column through upwelling (green) and basal mixing at the base of the wintertime mixed layer/T_{min} layer (blue), both of which are perennial. (a) During winter, the surface and T_{min} homogenize. (b) At the onset of summer, they separate into two layers due to surface warming and freshening. Although not shown here, the upper waters may also receive NO_3^- from lateral mixing with more polar waters (DiFiore et al., 2009). The intensity of gray shading qualitatively represents [NO_3^-].

age separation by providing a quantitative estimate of the decline in NO_3^- supply that was required during ice ages. To do so, we have developed a numerical model of N isotopes in the upper water column of the AZ that includes seasonally varying physical and biogeochemical processes. The model is tuned to modern conditions using estimates and observations of summertime NO_3^- drawdown, biomass abundance, export production, and upwelling. With this model, we quantify the proportion by which communication between the deep and surface must have decreased during ice ages to satisfy the coupled rise in $\delta^{15}N_{db}$ and decline in export production indicated by the downcore proxy measurements.

Our numerical model differs fundamentally from prior efforts to quantitatively interpret sedimentary $\delta^{15}N_{db}$ data. Previously, diatom-bound N isotope ratios were analyzed using the Rayleigh model, a set of analytical expressions for relating isotopic ratios to the fractional consumption of an initial substrate (François et al., 1997; Studer et al., 2015). In the context of Southern Ocean sediments, the Rayleigh model has been used to relate $\delta^{15}N_{db}$ to the degree of NO_3^- consumption in the summertime surface ocean and subsequently to estimate the ice age reduction in gross NO_3^- supply (François et al., 1997). However, the Rayleigh model must assume a concentration and $\delta^{15}N$ for the NO_3^- supply (i.e., for the NO_3^- in the surface prior to the spring/summer drawdown period). If the concentration of the NO_3^- supply and the depth of the mixed layer are held constant between interglacial and glacial cases, then the rise in $\delta^{15}N_{db}$ requires a rise in export production, violating observations.

In reality, the NO_3^- supply available for consumption during the summertime growth period is dependent on the degree of NO_3^- drawdown and other processes that occurred during the prior years. The nutrient dynamics of the AZ upper water column derive in large part from the seasonal cycle in vertical structure (Figure 1). In the winter, there is a single, ~175-m-deep wind-mixed layer (Figure 1a; Dong et al., 2008). Into the spring and summer, warming and freshening lead to the development of a ~50-m-deep mixed layer, with the deeper portion of the past winter's mixed layer below it (Figure 1b). This summertime shoaling of the mixed layer increases the average light conditions experienced by the phytoplankton within it, working with the increased flux of solar radiation to drive spring and summer phytoplankton growth (Mitchell et al., 1991; Smetacek & Passow, 1990). The development of a shallow summer mixed layer also isolates a shallow subsurface layer, known as the temperature minimum layer (T_{min}), which retains the low temperatures of the Antarctic winter (Sharma & Mathew, 1985). In the following autumn and winter, the previous summer's mixed layer is once again homogenized into the underlying waters, leading to the redevelopment of the winter mixed layer.

A key implication of the modern seasonality of the AZ upper water column is that wintertime mixed layer deepening does not return the surface layer to the NO_3^- concentration ([NO_3^-]) of the deep ocean. Rather, it returns it to a [NO_3^-] that is intermediate between the summertime surface and the deep waters below the wintertime mixed layer, with additional alteration by the remineralization of particulate N (PN) and ammonium (NH_4^+) that is resident in the late summer mixed layer when mixed layer deepening begins (Smart et al., 2015).

The Rayleigh model is inherently incapable of capturing the feedbacks between the degree of summertime NO_3^- consumption and the concentration and $\delta^{15}N$ of the NO_3^- available for consumption at the start of the spring-summer growth period. Thus, in previous work, it was not known to what degree the ice age $\delta^{15}N$ elevation of export production was due to a greater summertime increase in NO_3^- $\delta^{15}N$ versus a perennially higher NO_3^- $\delta^{15}N$ in the AZ above the base of the winter mixed layer (including in the spring-summer mixed layer inherited from the prior winter). Moreover, it could not be determined whether the higher degree of NO_3^- consumption was with respect to the ultimate deep ocean NO_3^- supply or the NO_3^- available at the beginning of seasonal NO_3^- drawdown. This, in turn, left great uncertainty in the glacial/interglacial change in the rate of gross NO_3^- supply from the deep ocean into the AZ upper water column. The model

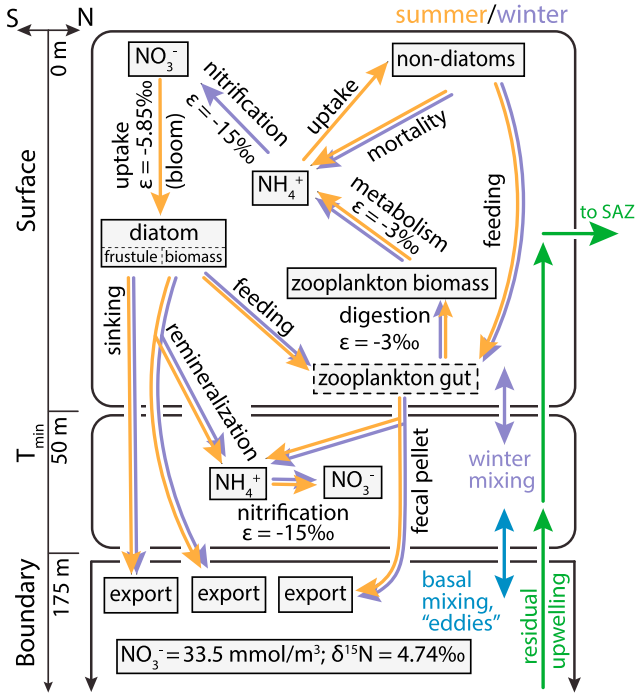

Figure 2. Model architecture. The surface layer contains NO_3^-, NH_4^+, diatoms, non-diatom phytoplankton, and zooplankton, and the subsurface layer contains NO_3^- and NH_4^+. NO_3^- is supplied through upwelling (green) and basal mixing (blue). Diatoms take up NO_3^- during the bloom portion of summer, and throughout the summer N is cycled among zooplankton, non-diatom phytoplankton, and NH_4^+ (orange arrows). In the winter (purple arrows), the surface and T_{min} homogenize. NH_4^+ is nitrified to NO_3^- throughout the year in the T_{min} layer, but only in wintertime in the surface layer. During the entire year, diatoms and zooplankton fecal pellets are exported from the surface ocean (although the flux is dominantly in the summer), and a fraction of exported diatom biomass and zooplankton fecal pellet N is remineralized in the T_{min} layer. Isotope effects ($^{15}\varepsilon$) are indicated for fractionating fluxes, rate constants for modern conditions are shown in Table 1, and model equations are given in supporting information S1.

developed here is intended to account for seasonally varying physical and biogeochemical processes in order to convert measurements of diatom-bound $\delta^{15}N$ to surface $[NO_3^-]$ and the rate of NO_3^- supply to the AZ surface at times in the past.

2. Seasonal Model of the Antarctic Zone

2.1. Model Description

2.1.1. Model Architecture

In order to capture the seasonal circulation and biogeochemistry of the AZ, the AZ model is comprised of two vertically arranged layers with summer and winter phases (Figure 2). In the model, the top layer represents the shallowest portion of the wind-mixed layer in winter and the entire mixed layer in summer, while the underlying layer represents the deeper portion of the mixed layer in the winter and the T_{min} layer in summer. We refer to the top layer as the *surface* and the lower layer as the *T_{min}*. The model parameterizes the surface mixed layer as having a depth of 50 m, and the base of the T_{min} layer is set at 175 m (Dong et al., 2008). Below the surface and T_{min} layers is an infinite reservoir of CDW, which interacts directly with the T_{min}.

In the surface, we track the concentration and $\delta^{15}N$ of N within NO_3^-, NH_4^+, diatoms, non-diatom phytoplankton, and zooplankton. Within the T_{min}, we track the concentration and $\delta^{15}N$ of NO_3^- and NH_4^+. The model is a series of differential equations, described in supporting information S1 and provided in Data Set S1, implemented in MATLAB and solved using the function *ode15s*. Briefly, diatom NO_3^- uptake follows a Monod parametrization (Sarthou et al., 2005), while most other biological fluxes have first-order dependence on substrate concentration. The concentrations and fluxes of NO_3^- and biomass N are calculated separately for ^{14}N and ^{15}N. Fluxes of ^{15}N are calculated based on those of ^{14}N accounting for the relevant isotope effect and the degree of substrate consumption at each model step (Hayes, 2004). As described below, the model calibration data are derived from profiles of $[NO_3^-]$ and NO_3^- $\delta^{15}N$ in the modern OAZ and PAZ (Kemeny et al., 2016). We compare model results to a sediment core from the OAZ (Studer et al., 2015). Accordingly, during the discussion of large-scale ocean biogeochemistry, we interpret the model as reflecting the southern limb of the upper cell of the global overturning circulation.

2.1.2. Water Exchanges

The model parameterizes two potential physical mechanisms of NO_3^- supply from CDW. The first path of NO_3^- supply is circumpolar westerly winds inducing the upwelling of deep water into the mixed layer (Figures 1 and 2 green arrows) and the northward transport of surface waters into the SAZ. This mechanism brings CDW into the T_{min} layer and water from the T_{min} into the surface, with water leaving northward from the surface layer. Conceptually, this upwelling is a component of the upper cell in the global overturning circulation (Toggweiler et al., 2006). The upwelling flux represents water that leaves the surface ocean at a different density than when it enters at the T_{min}/CDW boundary, so at the regional scale it is probably best compared to the upper cell of the Southern Ocean residual circulation, which is the net movement of water resulting from Ekman pumping after its partial compensation by the eddy-driven flow (Marshall & Speer, 2012). The second type of supply, which we term basal mixing (Figures 1 and 2 blue arrows), represents all other diapycnal, two-way exchanges between deep water and the base of the T_{min} layer. Furthermore, basal mixing potentially includes a contribution from both diapycnal mixing throughout the PAZ and the deep overturning occurring in the PAZ close to Antarctica that is typically described as directly ventilating the abyssal Antarctic; in this case, the NO_3^- supplied to the upper PAZ is communicated to the OAZ by lateral exchange (DiFiore et al., 2009, 2010). Because basal mixing represents the exchange of water parcels with different densities between the T_{min} layer and CDW, it also requires fluxes of buoyancy and so only

approximately represents the eddies commonly discussed in connection with the Southern Ocean residual circulation (Marshall & Speer, 2012). Upwelling from the T_{min} layer to the surface layer occurs throughout the year. The surface and T_{min} layers mix vigorously during the winter, but no summertime mixing is allowed between the two layers. While the seasonal model resolves the residual circulation and basal mixing as two distinct physical mechanisms of NO_3^- supply into the AZ, it cannot directly distinguish between their relative importance in the modern Southern Ocean or during the Last Glacial Maximum (LGM).

2.1.3. Biogeochemical Processes

The model parameterizes two summertime phases and one wintertime phase of biomass accumulation, mortality, and biogeochemical transformations (Figure 2). The summertime is split into two halves in order to represent the seasonal intensification of Fe limitation. The first 90 days of the summer, termed the bloom period, reflect rapid diatom growth in Fe-replete conditions. At the time of NO_3^- consumption, the model divides diatom-assimilated N into biomass and frustule-bound N. The latter half of the summer, termed the late summer period, reflects Fe-depleted conditions that halt diatom NO_3^- assimilation and cause a transition in phytoplankton growth from diatoms to non-diatoms and new production to recycled production (Sambrotto & Mace, 2000; Tagliabue et al., 2014). Regardless of season, each day, a fraction of diatoms is exported from the surface layer, and some exported diatom biomass is remineralized to NH_4^+ in the T_{min} layer. The model separately tracks the abundance and $\delta^{15}N$ of diatom biomass and frustules that reach the sediments.

Two cases are considered with regard to seasonal N cycling within the layers of the model: (1) no upper ocean N cycling and (2) active N cycling. The modern calibration is conducted with active N cycling, as it is an integral part of the complete model. In the case with no N cycle, zooplankton do not graze on diatoms and the only active biogeochemical processes are summertime NO_3^- assimilation by diatoms, remineralization of exported diatom biomass to NH_4^+ and then to NO_3^-, and export of diatom biomass and frustules to the sediments. In the case with an active N cycle, N is also cycled through zooplankton, NH_4^+, and non-diatom phytoplankton (Figure 2). Zooplankton export fecal pellets, which are also partially remineralized to NH_4^+ in the T_{min} layer, and the model tracks the flux and $\delta^{15}N$ of fecal pellets reaching the sediments separately from the export of diatom biomass and frustules. The model assumes that non-diatom phytoplankton are not directly exported from the surface ocean, which represents a simplification of unknown importance (Close et al., 2013; Fawcett et al., 2011; Michaels & Silver, 1988; Waite et al., 2000).

During all phases of the model, NH_4^+ in the T_{min} layer is nitrified to NO_3^- at a constant rate. Conversely, NH_4^+ in the surface ocean is only nitrified in the wintertime (Smart et al., 2015).

2.2. Model Calibration to Modern Conditions

The magnitudes of fluxes between N pools are manually tuned to match modern observations from the Southern Ocean surface, described below (Tables 1 and 2).

2.2.1. Summertime NO_3^- Depletion and Particulate Nitrogen Accumulation

The model is tuned to the concentration and $\delta^{15}N$ of $NO_3^- + NO_2^-$ that Kemeny et al. (2016) report for the late summer Pacific sector AZ (Table 2). Most of the profiles in this data set are underlain by LCDW, which minimizes the influence of lateral mixing between the T_{min} layer and poleward waters (DiFiore et al., 2009, 2010). Moreover, we limit the calibration to the $NO_3^- + NO_2^-$ data to avoid possible complications from N isotope equilibration between NO_3^- and NO_2^- (Kemeny et al., 2016); however, for simplicity, we use NO_3^- to refer to the combined $NO_3^- + NO_2^-$ reservoir. We take the AZ end-summer surface to have [NO_3^-] of 25.4 mmol/m^3 and NO_3^- $\delta^{15}N$ of 6.0‰, the T_{min} to have [NO_3^-] of 30.0 mmol/m^3 and NO_3^- $\delta^{15}N$ of 5.05‰, and CDW to have [NO_3^-] of 33.5 mmol/m^3 and NO_3^- $\delta^{15}N$ of 4.74‰. While these observations cannot be assumed to reflect the mean conditions of the whole AZ, they provide a fair representation of the region (DiFiore et al., 2010; Sigman et al., 1999; Smart et al., 2015).

Surface suspended PN is typically measured as the material that accumulates on filters. In the model, PN is represented as the sum of diatoms, non-diatom phytoplankton, and zooplankton. Although the model lacks specific bacterial and detrital particle pools, preliminary evidence indicates that these reservoirs are not highly distinct in $\delta^{15}N$ from non-diatom phytoplankton (Fawcett et al., 2011; Trull et al., 2015). The constraint on the model from measured PN concentrations ([PN]) limits the maximum accumulation of organic N and indirectly controls the timescales over which modeled biomass can accumulate. While [PN] can reach elevated values in coastal environments (Koike et al., 1986), we take the total [PN] in the open ocean to be

Table 1
Model Parameters to Recreate Modern Observations From the Antarctic Zone (Figures 3 and 4)

Model parameter	Value	$^{15}\varepsilon$	References
Length of model	150 years		
Length of summer	182 days		
Length of winter	183 days		
Diatom growing Season	first 90-days summer		
Antarctic Zone surface area	1.8×10^{13} m^2		Derived from Orsi et al. (1995)
Initial summer mixed layer depth	50 m		
Depth of T_{min} layer base	175 m		Dong et al. (2008)
Upwelling	4.8 cm/day		see discussion in text
Basal mixing	4.8 cm/day		see discussion in text
Circumpolar deep water [NO_3^-]	33.5 mmol/m^3		Kemeny et al. (2016)
Circumpolar deep water NO_3^- $\delta^{15}N$	4.74‰		Kemeny et al. (2016)
Diatom NO_3^- uptake;	57 μmol m^{-3} day^{-1}	−5.85‰	Capone et al. (2008)
V_{max} (top), $K_{1/2}$ (bottom)	500 μmol/m^3		Kemeny et al. (2016)
Diatom sinking	3%/day	0‰	calibrated to fit observations
Diatom frustule/total N ratio	0.1%		Takeda (1998); Hutchins and Bruland (1998); Claquin et al. (2002)
Diatom frustule/biomass fractionation		2.8‰	Morales et al. (2013, 2014)
Zooplankton diatom uptake	3%/day	0‰	calibrated to fit observations
Zooplankton non-diatom uptake	17%/day	0‰	calibrated to fit observations
Zooplankton digestion	95%/day	−3‰	Altabet and Small (1990)
Zooplankton metabolism	50%/day	−3‰	Checkley and Miller (1989)
Non-diatom NH_4^+ uptake	40%/day	0‰	calibrated to fit observations
Non-diatom mortality	3%/day	0‰	calibrated to fit observations
NH_4^+ nitrification	5%/day	−15‰	Casciotti et al. (2003)
Export remineralization	10%	0‰	Estimated from Weber et al. (2016); see supporting information S5 for 20%, −3‰

Note. Negative isotope effects favor processing of ^{14}N relative to ^{15}N.

~1 mmol/m^3 (e.g., DiFiore et al., 2009; Martiny et al., 2013). Lourey et al. (2003) record summertime suspended PN $\delta^{15}N$ ranging from ~1‰ to −5‰, a similar range as measured by Altabet and François (1994), the lower end of which Lourey et al. (2003) attribute to late summer N recycling. Due to lack of observational constraints from the AZ surface, the contribution of distinct biomass groups to [PN] remains a major uncertainty; for the purposes of calibrating the model, we estimate that the summertime concentration of diatoms reaches ~0.75–1.0 mmol/m^3 N, the concentration of non-diatom phytoplankton is ~0.75–1.0 mmol/m^3 N, and the concentration of zooplankton is ~0.25–0.50 mmol/m^3 N (Koike et al., 1986). The seasonal evolution of

Table 2
Comparison of Modern Observations and Modeled Fit

Observable	Model Results	Modern Observation	Reference
End-summer Surface [NO_3^-] (mmol/m^3)	25.25	25.4	Kemeny et al. (2016)
End-summer Surface NO_3^- $\delta^{15}N$ (‰)	6.03	6.0	Kemeny et al. (2016)
End-summer T_{min} [NO_3^-] (mmol/m^3)	30.32	30.0	Kemeny et al. (2016)
End-summer T_{min} NO_3^- $\delta^{15}N$ (‰)	5.02	5.05	Kemeny et al. (2016)
Maximum summer diatom (mmol/m^3)	0.93	0.75–1.00	
Maximum summer zooplankton (mmol/m^3)	0.34	0.25–0.50	
Maximum summer non-diatom (mmol/m^3)	0.97	0.75–1.00	
Maximum summer [NH_4^+] (mmol/m^3)	0.49	0.30–0.70	Bianchi et al. (1997)
		0.50–1.50	Sambrotto and Mace (2000)
Maximum winter [NH_4^+] (mmol/m^3)	0.72		
End-summer particulate nitrogen (mmol/m^3)	1.00	0.50–1.00	DiFiore et al. (2009)
		varied	Martiny et al. (2013)
End-summer suspended particulate nitrogen $\delta^{15}N$ (‰)	−5.08	~−5.0	Lourey et al. (2003)
Total export production (mmol/m^2)	165.3	100–500	Rubin et al. (1998)
Diatom/zooplankton export ratio	2.21	~2	Studer et al. (2015)

$[NH_4^+]$ is also uncertain. In the high-productivity Scotia Sea, $[NH_4^+]$ is observed to increase throughout the summer from ~0.2–0.35 mmol/m^3 in the spring (Olson, 1980) to ~0.5–1.5 mmol/m^3 during the late summer (Glibert et al., 1982; Rönner et al., 1983), but rising as high as 4.5 mmol/m^3 in coastal settings (Koike et al., 1986). In the open Indian sector of the Southern Ocean, Bianchi et al. (1997) observe late summer/early winter $[NH_4^+]$ ranging from 0.3 to 0.7 mmol/m^3, with stations south of the APF at the lower end of this range. Along 170°W, Sambrotto and Mace (2000) observe late summer $[NH_4^+]$ ranging from ~0.5 to 1.5 mmol/m^3 south of the APF, with a mean AZ value ~1 mmol/m^3. Recognizing that summertime changes in $[NH_4^+]$ remain uncertain, we parametrize the model to have an end-summer $[NH_4^+]$ of ~0.5 mmol/m^3. Estimates of AZ export production are in the range of ~100–500 mmol N m^{-2} $year^{-1}$ (Rubin et al., 1998), probably toward the lower end (Munro et al., 2015) but with higher values toward the coasts (Sweeney et al., 2000). Sinking PN $\delta^{15}N$ has been measured at ~0‰–2‰, which is significantly higher than suspended PN $\delta^{15}N$ (Altabet & François, 2001; Lourey et al., 2003).

In the results described below, the $\delta^{15}N$ of sinking PN approaches the higher end of the observed range. If we included isotope fractionation with remineralization of sinking PN in the T_{min}, the sinking PN $\delta^{15}N$ may exceed observations. However, a remineralization isotope effect would also retain ^{14}N in the upper ocean, allowing for a lower intensity of late summer N recycling and a lower $\delta^{15}N$ of export. In net, isotope fractionation during remineralization provides an alternative approach for generating modern N isotope observations (supporting information S5, Figure S14). In the main manuscript, however, we assume no fractionation during the remineralization of sinking PN (Altabet et al., 1991; Table 1).

2.2.2. Calibration of Water Exchanges

Because the model does not explicitly simulate eddy processes, its upwelling term represents the difference between the wind-driven Ekman pumping and the opposing eddy transport (Marshall & Speer, 2012). Although Ekman upwelling in the AZ is ~20 Sv (Karsten & Marshall, 2002), the residual transport is found to be only about 10–15 Sv (Abernathey et al., 2016; Karsten & Marshall, 2002; Marshall, 1997; Marshall et al., 2006; Marshall & Radko, 2003, 2006; Marshall & Speer, 2012; Sallée et al., 2010). The magnitude of upwelling per ocean area is the residual transport normalized to the surface area of the open AZ (i.e., between the APF and the Southern Boundary), calculated to be 1.8×10^{13} m^2 using the frontal positions of Orsi et al. (1995). Here we present results for modern upwelling of 10 Sv (i.e., 4.8 cm/day), consistent with the lower end of existing estimates.

In order to simultaneously match the target value for AZ export production and observations of seasonal surface $[NO_3^-]$, the model requires approximately 20 Sv of gross exchange between the T_{min} layer and the underlying deep ocean, roughly consistent with existing estimates (Abernathey et al., 2016). Given the evidence for approximately 10 Sv of residual upwelling, the 10 Sv of additional gross exchange with deep water that is required is parameterized as basal mixing. Importantly, model results are similar for 20 Sv of upwelling and 0 Sv of basal mixing, or for 20 Sv of basal mixing and 0 Sv of upwelling (supporting information S3, Figures S3–S9).

2.2.3. Calibration of Biogeochemical Processes

During the bloom period of the summertime, diatoms assimilate NO_3^- with a normal isotope effect of −5.85‰. Diatom assimilation of NO_3^- follows Monod kinetics where the half-saturation constant and maximum uptake rate are 500 μmol/m^3 and 57 μmol m^{-3} day^{-1}, respectively (Capone et al., 2008). Practically, diatoms consume NO_3^- at the maximum uptake rate each day during the bloom period until $[NO_3^-]$ becomes very low, which only occurs in the experiments approximating the ice age separation hypothesis, with low NO_3^- supply. During the late summer period and the wintertime, diatoms do not assimilate NO_3^-. On each day, regardless of the season, 3% of the diatom pool is exported from the surface ocean.

In simulations with N cycling, zooplankton consume 3% of the diatom pool and 17% of the non-diatom phytoplankton pool each day. To represent digestion, zooplankton assimilate 95% of this incoming food into biomass with a −3‰ isotope effect and release the remainder as fecal pellets (Altabet & Small, 1990). To represent metabolism, zooplankton release as NH_4^+ 50% of their biomass each day with an isotope effect of −3‰ (Altabet & Small, 1990; Checkley & Miller, 1989). The two equal isotope effects of digestion and metabolism do not mutually cancel because the fractional input of N during digestion (95%/day, with zooplankton as the product pool) is significantly larger than the fractional output of NH_4^+ during metabolism (50%/day, with zooplankton as the substrate pool); when considering the influence of digestion and metabolism on the isotopic composition of zooplankton relative to their food source, the isotope effect of metabolism is

more fully expressed than the fractionation associated with digestion. This combination of digestive and metabolic processes forces the $\delta^{15}N$ of zooplankton to stay elevated relative to the $\delta^{15}N$ of their food source (DeNiro & Epstein, 1981; Fry, 1988; Minagawa & Wada, 1984; Wada et al., 1987) while also forming fecal pellets elevated in $\delta^{15}N$ relative to the food source (Altabet & Small, 1990). Grazing by zooplankton and their release of high-$\delta^{15}N$ fecal pellets and low-$\delta^{15}N$ NH_4^+ results in the accumulation of low-$\delta^{15}N$ N in the surface mixed layer within the NH_4^+ and non-diatom phytoplankton reservoirs. Non-diatom phytoplankton consume 40% of the available NH_4^+ daily with an isotope effect of 0‰ and release 3% of their biomass to the NH_4^+ pool each day without fractionation. This value is unlikely to be the actual isotope effect of NH_4^+ assimilation at the conditions present in the AZ surface (Vo et al., 2013), but the low [NH_4^+] and the fact that, in the summer, only assimilation consumes the surface mixed layer NH_4^+ pool causes this isotope effect assignment to have only minor significance for the model output. Non-diatom phytoplankton are assumed to assimilate only NH_4^+, not NO_3^-, and only during the summer. In simulations with an active N cycle, the consumption of diatoms and non-diatom phytoplankton by zooplankton and the consumption of NH_4^+ by non-diatom phytoplankton occur during both the diatom-bloom and postbloom phases of the summertime. NH_4^+ remaining at the end of the summer in the surface is nitrified to NO_3^- at a rate of 5% daily with an assumed isotope effect of −15‰ (Casciotti et al., 2003), and NH_4^+ in the T_{min} layer is nitrified during both summer and winter at the same rate and with the same isotope effect. While the isotope effect of nitrification is uncertain, the high degree of NH_4^+ consumption by nitrification and the lack of significant competition from other processes cause the choice for this isotope effect to have no significant impact.

Ten percent of N exported from the surface ocean as diatom biomass or zooplankton fecal pellets is remineralized to NH_4^+ in the T_{min} layer, although this value is poorly constrained and has been demonstrated to vary spatially (Berelson, 2001; Martin et al., 1987; Weber et al., 2016). N bound within diatom frustules is not remineralized. As further discussed below, we assume an isotope effect of 0‰ for the remineralization of organic matter in the T_{min} layer (supporting information S5).

2.3. Modeling Glacial Conditions and $\delta^{15}N_{db}$

2.3.1. Simulation of Ice Age Conditions

In modeling of ice age conditions, reductions in the gross NO_3^- supply to the surface ocean are simulated with simultaneous and equal reductions in upwelling and basal mixing (Figure 2). Relative to the interglacial case of 20 Sv, these reductions decrease the movement of water across the base of the T_{min} layer/winter mixed layer, reducing the total amount of N in the surface ocean. The decision to apply equal reductions in upwelling and basal mixing reflects our uncertainty in the relative strength of these two NO_3^- supply mechanisms throughout the last glacial cycle. Moreover, the magnitude of basal mixing may depend in part on the strength of upwelling (Abernathey & Ferreira, 2015), such that simultaneous reductions in both mechanisms are plausible. Finally, for the purposes of quantifying the reduction in deep-surface exchange required to explain paleoceanographic measurements, equal reduction of upwelling and basal mixing is a more conservative choice than a reduction in upwelling alone.

In a subset of model simulations, a reduction in the summertime mixed layer depth is included that occurs in proportion with the decline in water (and NO_3^-) supply from below, reaching a minimum summertime mixed layer depth of 25 m. In these simulations the wintertime mixed depth remains 175 m. Shoaling the wintertime mixed layer in parallel with the summertime mixed layer had no significant effect (results not shown). The water fluxes and thus the gross supply of NO_3^- from deep water are not affected by changes in mixed layer depth. Results for ice age simulations are presented in the main text, and additional model output from this set of simulations is given in supporting information S4 (Figures S11–S13).

2.3.2. Comparison of Measured and Simulated $\delta^{15}N_{db}$

A central purpose of this study is to relate the model output for diatom biomass $\delta^{15}N$ with observations of $\delta^{15}N_{db}$ from sediment cores, and below we compare our model output to the data of Studer et al. (2015). However, to compare simulated biomass $\delta^{15}N$ with the $\delta^{15}N$ of N protected and preserved within diatom frustules, we need to account for the distinction between bulk diatom biomass and the N bound within the diatom frustules that accumulate in the sediment. The culture study of Horn et al. (2011) suggests that $\delta^{15}N_{db}$ is typically lower than biomass $\delta^{15}N$, with significant taxonomic variation. In contrast, a cleaning protocol study by Morales et al. (2013) and a Bering Sea net tow study by Morales et al. (2014) both suggest a 2‰–3‰ elevation in the $\delta^{15}N$ of frustule-bound N relative to diatom biomass. The elevation of $\delta^{15}N_{db}$

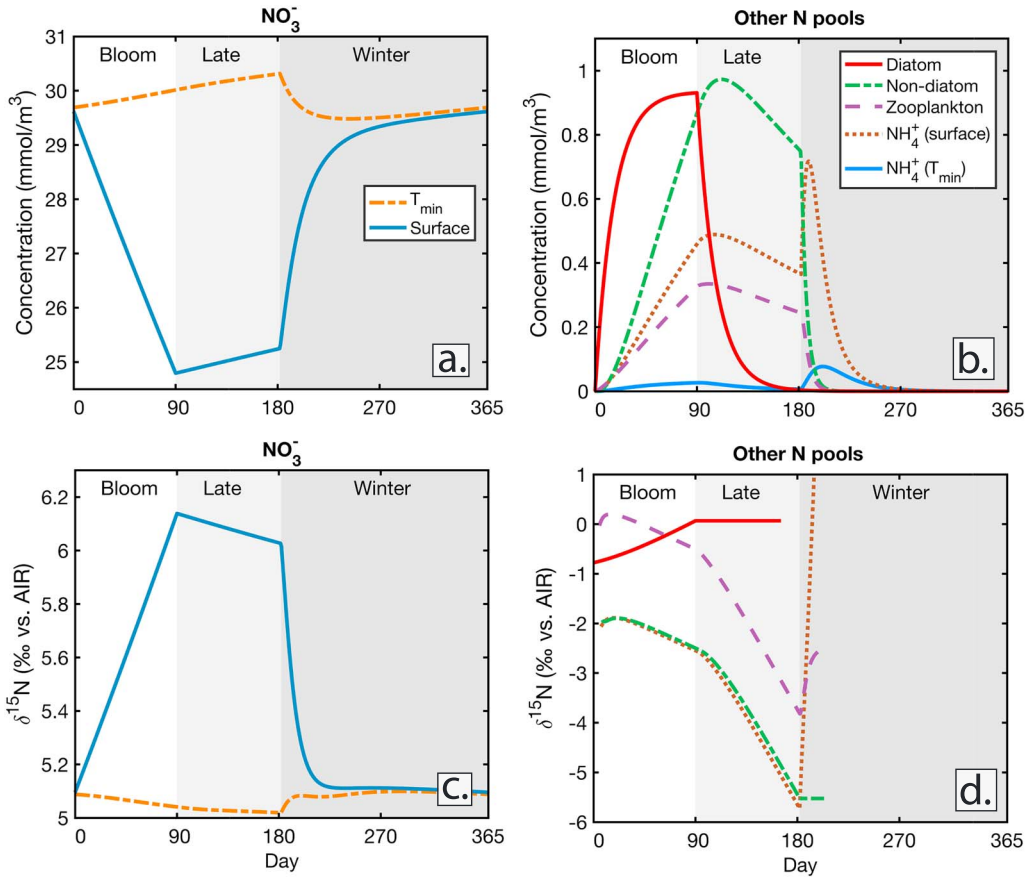

Figure 3. Steady state model results tuned to modern conditions. For the bloom portion of summer (white, "Bloom"), diatoms consume NO_3^- and zooplankton consume diatoms and non-diatom phytoplankton. Zooplankton release NH_4^+, which is cycled through non-diatom phytoplankton. During the late summer (light gray, "Late"), recycled production dominates and the $\delta^{15}N$ of suspended PN declines. During winter (dark gray, "Winter"), the surface and T_{min} layers homogenize, diatoms and non-diatom phytoplankton do not assimilate N and are consumed without fractionation, and NH_4^+ is nitrified to NO_3^- in the surface and T_{min} layers. $\delta^{15}N$ values are plotted for all pools with N content >0.01 mmol/m^3. Analogous model results for the midglacial and glacial scenarios are given in supporting information S2 (Figures S1 and S2).

relative to diatom biomass is consistent with the difference observed between the $\delta^{15}N$ of NO_3^- consumed in surface waters with sediment core top $\delta^{15}N_{db}$ in both the Antarctic and the subarctic North Pacific (Brunelle et al., 2007; Robinson et al., 2004), so we favor that field-based finding. For purposes of comparing our modeled export production with actual observations, when partitioning consumed N into diatom biomass and frustule components we assume the frustule-bound N to be 2.8‰ higher in $\delta^{15}N$ than the diatom biomass. However, we stress that the model's output is more meaningful for its changes in $\delta^{15}N_{db}$ than for its absolute values. Importantly, downcore variation in diatom taxa is minor in the sediment core of Studer et al. (2015), such that species differences in the $\delta^{15}N$ offset between biomass and frustule cannot explain the downcore $\delta^{15}N_{db}$ variations. This assertion is further supported by assemblage specific $\delta^{15}N_{db}$ records reported by Studer et al. (2015).

3. Results and Discussion

3.1. Seasonality in the Modern Southern Ocean Surface

The model achieves an interannual steady state for modern conditions and glacial simulations within 150 years, and we exclusively consider model output after steady state is achieved. During the bloom phase of summer, diatoms assimilate NO_3^-, decreasing surface ocean [NO_3^-] and causing progressive summertime increases in both surface NO_3^- $\delta^{15}N$ and diatom $\delta^{15}N$ (Figure 3, no shading). Zooplankton consume both diatoms and non-diatom phytoplankton, preferentially digesting ^{14}N and shunting ^{15}N to fecal pellets.

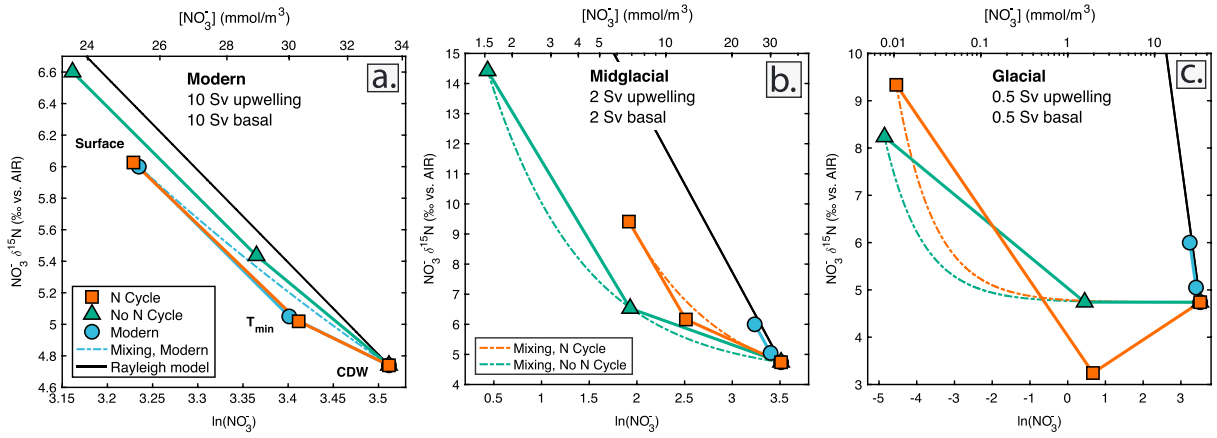

Figure 4. The concentration and $\delta^{15}N$ of NO_3^- in the surface ocean, the T_{min} layer, and Circumpolar Deep Water (CDW) from modern observations (blue circles, Kemeny et al. (2016)), the model with (orange squares) and without (green triangles) an active nitrogen cycle, and mixing curves (dash-dot) between surface water and CDW. (a) In the modern simulation (20 Sv of CDW supply), the model recovers the isotopic structure measured in the upper water column of the Antarctic Zone. The simulation without a N cycle falls off the Rayleigh model due to mixing dynamics. However, it does not produce a strong low-$\delta^{15}N$ variation from Rayleigh expectations, suggesting that observations from the modern T_{min} layer results from biological N cycling and PN nitrification (supporting information S5). (b) In the midglacial case (4 Sv of supply), surface NO_3^- $\delta^{15}N$ increases as CDW supply is reduced. In the T_{min}, NO_3^- $\delta^{15}N$ increases as NO_3^- with elevated $\delta^{15}N$ is incorporated from the surface during wintertime mixing. The deviation from Rayleigh expectations in the model without an active N cycle is entirely attributable to mixing (green dash-dotted curve). With the N cycle, the deviation from the Rayleigh model is produced by a combination of mixing effects and the isotopic impact of N cycling. (c) During peak glacial conditions (1 Sv of supply), T_{min} NO_3^- $\delta^{15}N$ declines to the value of CDW in the simulation without a N cycle and declines below the CDW value in the model with a N cycle. For comparison and to highlight the differences in axes among panels, we show the modern observations (blue circles) in all three panels. For NO_3^- assimilation, both the seasonal model and Rayleigh calculation use an isotope effect of −5.85‰.

Zooplankton then release low-$\delta^{15}N$ NH_4^+, which is cycled through the NH_4^+ and non-diatom phytoplankton reservoirs before passing back to zooplankton through the consumption of non-diatom phytoplankton. In the late summer phase, when diatom growth is not permitted, zooplankton, NH_4^+, and non-diatom phytoplankton decline in $\delta^{15}N$ as N is cycled within the summer mixed layer without replenishment from newly assimilated NO_3^- and relatively ^{15}N-rich N is lost as fecal pellets (Figure 3, light gray shading). With the input parameters in Table 1, diatoms grow to 0.93 mmol/m^3 in the summertime surface, zooplankton increase to 0.34 mmol/m^3, non-diatom phytoplankton build to 0.97 mmol/m^3, and [NH_4^+] reaches 0.49 mmol/m^3 (Table 2). In the late summer surface, [NO_3^-] increases and NO_3^- $\delta^{15}N$ decreases due to CDW input by continuous upwelling and basal mixing. In the T_{min}, [NO_3^-] rises and NO_3^- $\delta^{15}N$ falls over the entire summer, due to NO_3^- supply from below as well as the remineralization of sinking organic matter.

Vigorous wintertime mixing homogenizes [NO_3^-] and NO_3^- $\delta^{15}N$ between the surface and the T_{min} layer (Figure 3, dark gray shading). Throughout the winter, upwelling of CDW increases [NO_3^-] and decreases the $\delta^{15}N$ of NO_3^- in the combined surface and T_{min} layers, which are homogenized at that time. The concentrations of biomass pools decrease in winter as organisms die without replenishment. Because diatoms and non-diatom phytoplankton are consumed without fractionation during the winter and do not assimilate N (Figure 2), the $\delta^{15}N$ of diatoms and nondiatom phytoplankton equal their end-summer values throughout the winter. Model results for modern conditions recover the observed [NO_3^-] and NO_3^- $\delta^{15}N$ structure of the upper water column (Figure 4a and supporting information S5) and approximately fit modern observations of biomass abundance (Table 2).

3.2. Ice Age Simulations: Reducing Gross NO_3^- Supply

3.2.1. Model N Isotopes

Ice age Antarctic separation was simulated by decreasing NO_3^- supply to the surface ocean through equal reductions in upwelling and basal mixing (Figure 5); however, our results change minimally if only one of these supply mechanisms is reduced (supporting information S3 and Figures S3–S9). Diatoms in the model consume NO_3^- at a roughly constant rate until [NO_3^-] becomes very low, as determined by the half-saturation constant governing the Monod representation of diatom growth (Table 1). As a result, decreasing the nutrient supply in model simulations with a constant mixed layer depth initially has a minimal impact on

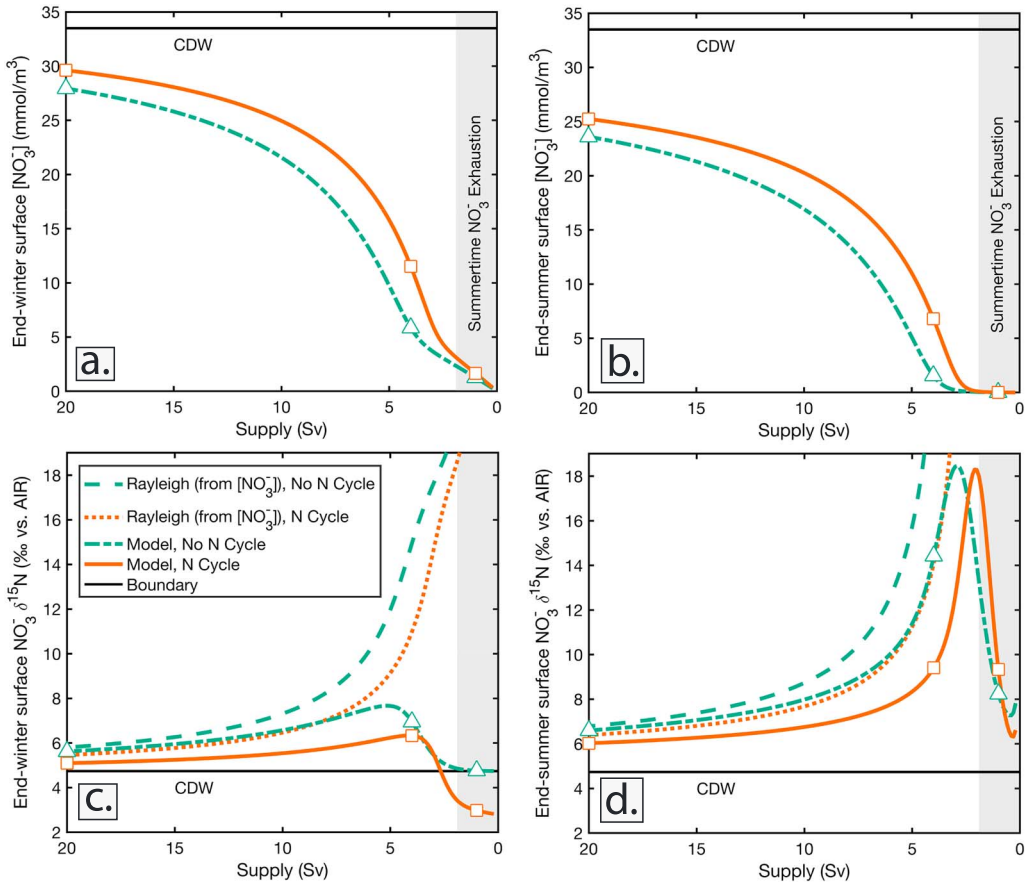

Figure 5. End-winter and end-summer surface $[NO_3^-]$ and NO_3^- $\delta^{15}N$ plotted against NO_3^- supply (i.e., Circumpolar Deep Water (CDW) gross input) for model results with and without an active N cycle (orange solid and green dash-dotted curves, respectively). (a, b) End-season $[NO_3^-]$ declines with reduced CDW supply and reaches exhaustion first in the model without an active N cycle. (c, d) End-winter and end-summer NO_3^- $\delta^{15}N$ in the mixed layer increase with lower CDW supply, but at a rate significantly lower than predicted from the Rayleigh model (orange dotted and green dashed lines). At very low degrees of CDW supply, end-season surface NO_3^- $\delta^{15}N$ declines. Symbols indicate the modern, mid-glacial, and glacial scenarios shown in Figure 4, and the black line indicates the $[NO_3^-]$ and NO_3^- $\delta^{15}N$ of CDW.

export production but increases the fractional consumption of NO_3^- during the summertime season (Figures 6a and 6b). In simulations with variable mixed layer depths, decreasing the nutrient supply reduces export production while also increasing the fractional consumption of NO_3^- (Figures 6c and 6d). In both cases, the increase in degree of NO_3^- consumption (Figures 5a and 5b) causes an increase in the $\delta^{15}N$ of both NO_3^- remaining in seawater at the end of summer (Figure 5d) and in exported diatoms (Figures 6b and 6d). For moderate declines in upwelling and basal mixing, the $\delta^{15}N$ of end-winter surface NO_3^- rises due to the higher $\delta^{15}N$ of the NO_3^- that is left in the summer surface layer following diatom NO_3^- assimilation. However, with still greater reductions in the rate of NO_3^- supply, despite the continued increase in $\delta^{15}N$ of the residual summertime surface NO_3^-, there is a decline in the end-winter $\delta^{15}N$ of surface NO_3^- (Figures 5c and 5d), as discussed further below.

For both winter and summer, the modeled $\delta^{15}N$ of surface NO_3^- is substantially lower than predicted by the Rayleigh model, with the difference becoming greater at lower $[NO_3^-]$ (Figure 5c and 5d). Focusing on the $\delta^{15}N$ of surface NO_3^- in the winter, the reason for these findings is that while the $\delta^{15}N$ of the residual surface NO_3^- continues to increase with greater fractional consumption of supplied nutrients, the $[NO_3^-]$ of the surface water that mixes downward during the winter becomes lower at decreased magnitudes of NO_3^- supply, thereby weakening the impact of the summertime surface layer on the NO_3^- $\delta^{15}N$ of the T_{min} layer. As NO_3^- supply is further decreased and summertime NO_3^- consumption proceeds almost to completion, the $\delta^{15}N$ of

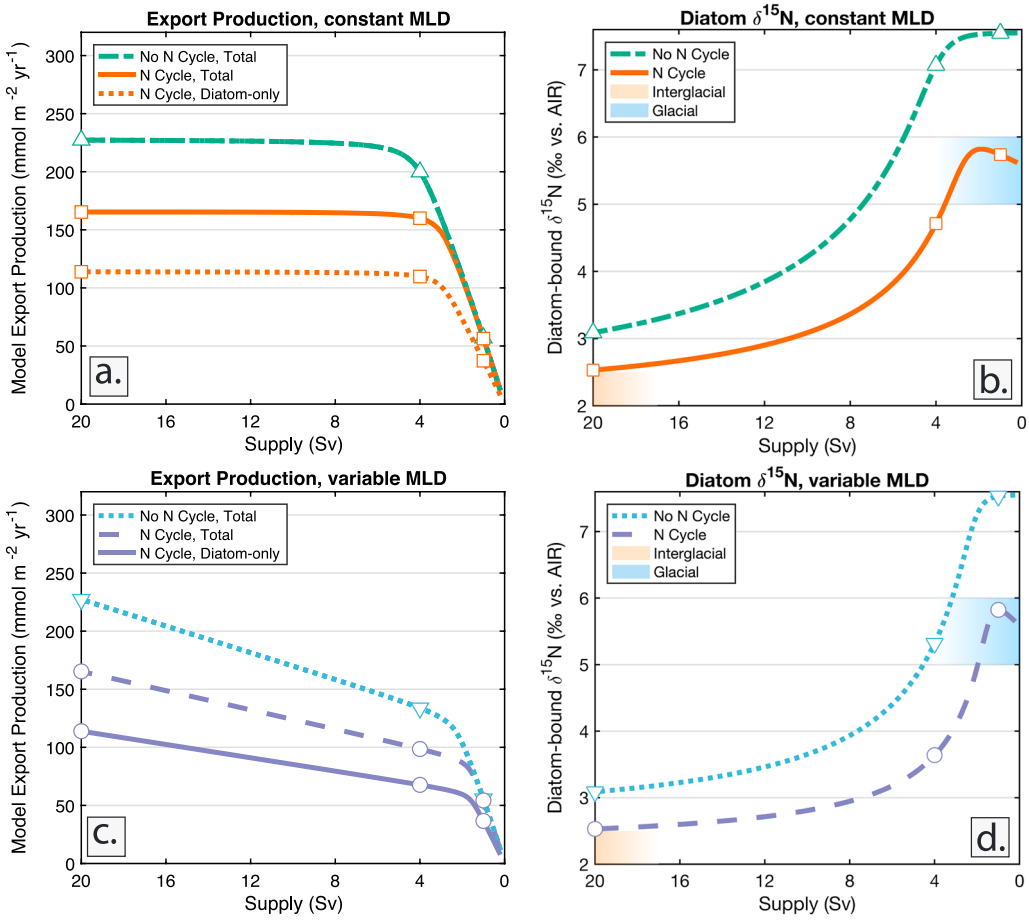

Figure 6. (a, c) Total and diatom-only export production and (b, d) diatom-bound $\delta^{15}N$ for models with (orange solid/dotted and purple dashed/solid curves) and without (green dashed-dotted and blue dotted curves) an active N cycle, for models with (a, b) constant mixed layer depth or (c, d) variable mixed layer depths. In simulations with a constant mixed layer depth, export production declines only at low rates of Circumpolar Deep Water (CDW) supply, while $\delta^{15}N_{db}$ increases with reduced CDW supply until very low rates. In simulations with a variable mixed layer depth, export production declines with CDW supply as $\delta^{15}N_{db}$ increases. Symbols indicate the modern, midglacial, and glacial scenarios shown in Figures 4 and S11. Orange and blue shaded regions reflect δ^{15}Ndb measurements from interglacials and glacials, respectively (Studer et al., 2015).

the T_{min} layer decreases toward the NO_3^- $\delta^{15}N$ of the waters upwelled or mixed upward from CDW, as does the NO_3^- $\delta^{15}N$ of the end-winter surface ocean (Figure 5c). Our results exemplify the underexpression of isotope effects associated with NO_3^- consuming processes that is common in the ocean and, more broadly, in the environment in general (Deutsch et al., 2004; Houlton et al., 2006; Thunell et al., 2004). The $\delta^{15}N$ of surface NO_3^- in the summer responds similarly to declining NO_3^- supply (Figure 5d). In the scenario without a N cycle, as the gross input of water from below decreases below ~2.5 Sv, surface NO_3^- becomes nearly exhausted during the summertime, and end-summer surface NO_3^- $\delta^{15}N$ declines toward the NO_3^- $\delta^{15}N$ of the waters upwelled from the T_{min} layer (Figure 5d, gray shading).

In the model case with active N recycling, at very low rates of NO_3^- supply, the $\delta^{15}N$ of wintertime NO_3^- in the mixed layer is lower than that of either CDW or the modern wintertime mixed layer (Figure 5). This is because, with active N recycling in the summer mixed layer, a low-$\delta^{15}N$ PN pool develops. In the winter, this PN is mixed throughout the wintertime mixed layer and generates low-$\delta^{15}N$ NO_3^- following remineralization and nitrification (Smart et al., 2015). As the gross NO_3^- supply from CDW into the wintertime mixed layer is decreased, this low-$\delta^{15}N$ regenerated NO_3^- becomes a more important influence on the NO_3^- $\delta^{15}N$, causing wintertime NO_3^- $\delta^{15}N$ to decrease below the $\delta^{15}N$ of the NO_3^- supply.

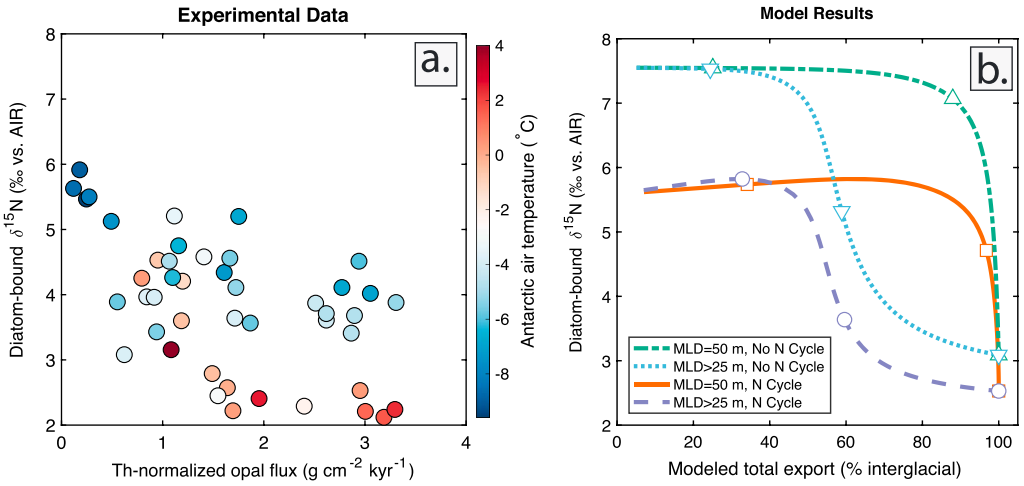

Figure 7. Measured and modeled diatom export and $\delta^{15}N$. (a) Measurements show a decline in diatom export and increase in $\delta^{15}N_{db}$ coincident with lower Antarctic air temperature. (b) Conversely, model results with a constant mixed layer depth both with (orange solid curve) and without (green dash-dotted curve) an active N cycle show increasing $\delta^{15}N$ without a significant decline in exported biomass, export production decreasing only when NO_3^- in the surface ocean is nearly exhausted. As a result, for a given value of $\delta^{15}N_{db}$, the model underestimates the relative change in export production. Thus, if export production proxy data are included in the model/data comparison, they argue for a greater reduction in Circumpolar Deep Water (CDW) supply than otherwise. Model results with variable mixed layer depths both with (purple dash curve) and without (blue dotted curve) a N cycle show increasing $\delta^{15}N$ with a corresponding decline in exported biomass. In (b), symbols, purple circles, and blue downward triangles indicate the modern, midglacial, and glacial scenarios shown in Figures 4 and S11. Observations of $\delta^{15}N_{db}$ and Th-normalized flux are from Studer et al. (2015) binned into 2 kyr intervals and color coded by interpolated Antarctic air temperature (Jouzel et al., 2007).

The concentration and $\delta^{15}N$ of NO_3^- in the wintertime mixed layer largely set the starting values for the summer mixed layer. Thus, the generally weak change in NO_3^- $\delta^{15}N$ of the winter mixed layer as its [NO_3^-] declines has great importance for the amplitude of the rise in diatom-bound $\delta^{15}N$ in response to the reduction in gross NO_3^- supply. Because mixing and PN remineralization/nitrification (the latter in the case of simulations with an active N cycle) depress the $\delta^{15}N$ of the winter mixed layer and reduce the $\delta^{15}N$ of the NO_3^- present at the start of the summer, a large reduction in the NO_3^- supply is required to explain the observed rise in $\delta^{15}N_{db}$. Specifically, in the model cases with upper ocean N cycling, a ~3‰–4‰ rise in $\delta^{15}N_{db}$ requires a >80% reduction in the gross NO_3^- supply from CDW (Figure 6b, orange solid curve, and Figure 6d, purple dashed curve). In the case without a N cycle, attaining the ice age increase in $\delta^{15}N_{db}$ requires only a >60% reduction in the gross NO_3^- supply from CDW (Figure 6b, green dash-dotted curve, and Figure 6d, blue dotted curve). However, the scenario lacking a N cycle does not adequately recreate modern observations in the T_{min} layer (Figure 4a and supporting information S5), supporting our focus on the model including the simulation of the upper ocean N cycle.

3.2.2. Export Production

In the model case with no N cycling, export production is entirely composed of diatom biomass (Figure 6a, green dashed curve, and Figure 6c, blue dotted curve), frustule-bound N representing a minor component of this. With N cycling, more than two thirds of the total organic N export is as diatom biomass, and the remainder as zooplankton export represented by fecal pellets. As most paleoceanographic measurements are of the accumulation rate of diatom-dominated biogenic opal, we focus here on the diatom component of the modeled export production. In the model with a constant mixed layer depth, diatom export holds nearly constant as the rate of gross NO_3^- supply declines (Figure 6a). This is the consequence of using a Monod function for NO_3^- assimilation and a low half-saturation constant (Table 1). Once [NO_3^-] falls below the half-saturation constant, diatom growth is sharply curtailed (Figure 6a).

The insensitivity of NO_3^- assimilation rate to all but the lowest [NO_3^-] is intended to reflect the fact that phytoplankton growth in the AZ surface is limited by Fe and/or light, which is supported by laboratory and field studies of phytoplankton. Moreover, at a qualitative level, it is supported by the paleoceanographic evidence for an increased degree of NO_3^- consumption in the AZ during the glacials, which requires that export

production declined less than did the NO_3^- supply (Studer et al., 2015). In detail, however, paleoceanographic proxy data for export production (Figure 7) indicate that there was a gradual decline in export production as NO_3^- supply decreased from interglacial levels, which the model with a constant mixed layer depth does not capture.

We attribute this inconsistency to the model's simplistic treatment of the controls on diatom growth, which does not explicitly include the role of Fe and light limitation. If upwelling CDW maintained a constant [Fe]/[NO_3^-] ratio over glacial cycles, then the supply rates of Fe and NO_3^- would change in constant proportion. In this case and assuming simple Fe limitation of diatom growth, export production would covary continuously with the rate of NO_3^- supply (Lefèvre & Watson, 1999). Importantly, this scenario also cannot be considered complete and accurate, as it would lead to perfectly covarying NO_3^- supply and export production and thus no change in the degree of NO_3^- consumption, which violates the $\delta^{15}N_{db}$ evidence for increased NO_3^- consumption during ice ages. One potential modification to this scenario is that there is significant augmentation of Fe supply from the atmosphere and the margins, such that decreasing the nutrient supply from CDW would lead to a rise in the Fe/NO_3^- supply ratio to the summertime mixed layer (Studer et al., 2015). Alternatively, Fe recycling in the surface ocean may lead to more NO_3^- drawdown than expected from the Fe/NO_3^- supply ratio, an effect that becomes more important as upwelling rate declines (Rafter et al., 2017). If the supply of NO_3^- and Fe to the AZ surface declined during ice ages, Fe recycling would allow for an increase in the degree of NO_3^- consumption. Regardless of the specifics, the existing coupled $\delta^{15}N_{db}$ and export production data would argue that export production did covary continuously with NO_3^- supply, in contrast to the model output when a constant mixed layer depth is assumed.

Model simulations with variable mixed layer depths fit the coupled $\delta^{15}N_{db}$ and export production proxy data somewhat better (Figures 6c, 6d, and 7b, purple dashed and blue dotted curves). In these simulations, the AZ summertime mixed layer depth is decreased in proportion with the decline in supply toward a minimum mixed layer depth of 25 m. While generating an immediate and continued reduction in export production (Figure 6c), these simulations yield $\delta^{15}N_{db}$ values comparable to those in the case of a constant mixed layer depth (Figure 6d). Our observations are again attributable to the Monod parametrization of diatom NO_3^- assimilation. Because NO_3^- consumption is only a function of ambient [NO_3^-] but export production scales with mixed layer depth, a shoaled mix layer has a large impact on the magnitude of N export but only impacts the degree of NO_3^- consumption indirectly. The major impact of the shoaled mixed layer on $\delta^{15}N_{db}$ is that relatively more CDW passes through the volume of the mixed layer, keeping AZ surface [NO_3^-] elevated and NO_3^- $\delta^{15}N$ depressed relative to the case with a constant, deeper mixed layer. As discussed above, we assume that the lack of an explicit Fe cycle compromises the model's simulation of diatom growth. Nevertheless, these model simulations including a variable mixed layer appear more consistent with the paleoceanographic observations, arguably offering support for mixed layer shoaling under glacial conditions of reduced NO_3^- supply.

In simulations with constant and variable mixed layer depths, we can compare peak glacial conditions with the lowest rates of exchange explored with the model. The Antarctic paleoproxy data appear to require that diatom export was at least 50% reduced during the glacial maxima; opal burial rates are observed to decline far more than this (Anderson et al., 2009; Jaccard et al., 2013; Kohfeld et al., 2005; Mortlock et al., 1991). The combination of a ~3‰–4‰ increase in $\delta^{15}N_{db}$ and a ≥50% decline in diatom export during peak glacial periods requires an ice age reduction of gross NO_3^- flux into the model's upper ocean layers from the underlying deep ocean (Figure 7) that is even more dramatic than when only considering the $\delta^{15}N_{db}$ increase (Figure 6). Such a large decrease, of 90% or more, has major implications for ice age ocean circulation. It appears to require a greatly reduced wind-driven upwelling, and probably also a decline in basal mixing.

4. Implications

4.1. Relationship to Prior Calculations

In large part, these results are consistent with the conclusions of François et al. (1997) for the AZ. These authors interpreted a rise in bulk sediment $\delta^{15}N$ of 2‰ using the Rayleigh model to estimate that glacial NO_3^- consumption was 70% of the gross NO_3^- supply. Using this finding and an estimate of the decline

in export production within a steady state framework, François et al. (1997) estimated a tenfold ice age reduction in the supply of water to the surface of the Southern Ocean south of the APF.

However, it is important to recognize the extreme limitations and uncertainties of this Rayleigh-based calculation. In particular, this model assumes no change in the $\delta^{15}N$ or concentration of NO_3^- prior to each growing season. Thus, this calculation inherently requires an increase in NO_3^- assimilation (and thus export production) in order to reach the higher degree of NO_3^- consumption implied by the $\delta^{15}N$ measurements, which is contradicted by the export production proxies. If François et al. (1997) had assumed a lower wintertime [NO_3^-] to attempt to simulate the glacial decrease in export production and used the Rayleigh model to calculate the initial $\delta^{15}N$ for that NO_3^-, then a lower degree of summertime NO_3^- consumption would have been required to match the $\delta^{15}N$ for export production (Figure 5). This would then have contradicted or reduced the need for more complete summertime NO_3^- consumption in order to drive the decrease in wintertime [NO_3^-]. In summary, the Rayleigh framework cannot provide a self-consistent picture of seasonality in the glacial AZ. Even if it could, it would not simulate the impacts of changing degrees of NO_3^- consumption on the mixing of water masses or the effects of remineralization on the $\delta^{15}N$ of the NO_3^- in the AZ upper water column. These failures motivated the construction and application of the numerical model discussed here.

The model indicates that the high $\delta^{15}N$ of N export during the glacials was mostly the consequence of a rise in NO_3^- $\delta^{15}N$ over the summer, with little increase in the $\delta^{15}N$ of wintertime NO_3^- that is available to phytoplankton at the beginning of the growing season. That is, the model demonstrates that wintertime NO_3^- $\delta^{15}N$ falls far below the relationship with NO_3^- concentration defined by the Rayleigh or steady state models. The net result is a self-consistent picture of seasonality in the glacial AZ and thus defensible estimates of winter and summer surface NO_3^- concentrations and of the gross rate of NO_3^- supply.

4.2. Slowing of the Residual Circulation of the Upper Cell

Our model results indicate that observed increases in diatom-bound $\delta^{15}N$ and declines in diatom export, taken together, require a reduction in gross water supply (upwelling plus basal mixing) from CDW to the upper AZ. Conservatively, the reduction in gross water supply is >80% during the LGM in the model with a N cycle and >60% in the model without a N cycle. Existing calculations of the residual circulation suggest 10 Sv as a rough lower limit on the required rate of residual upwelling in the Antarctic, whereas total Ekman divergence is estimated at 20 Sv (Karsten & Marshall, 2002). Accordingly, the model control case was developed with 10 Sv each of upwelling and basal mixing, recognizing that this might underestimate the role of the former. Prior to this study, it was unclear whether the LGM reduction in NO_3^- supply required a decline in upwelling, basal mixing, or both. The model's indication of the need for a >80% decline in total supply during the LGM requires a reduction in upwelling. This upwelling is the central component of the upper cell of Southern Ocean overturning, and our results thus point to a reduction in this upper cell.

4.3. Physical Mechanism

Most of the water upwelled in the open AZ is destined to flow northward toward the APF. Thus, our interpretation of an ice age decline in AZ upwelling likely requires a reduction in net northward transport of AZ surface waters toward the APF. Current theory stresses that the upper cell, composed of the net upwelling and northward surface water transport in the Antarctic, reflects the residual of the two countervailing processes of Ekman pumping and the eddy response to the resulting isopycnal tilting (Figure 8a; Marshall & Speer, 2012). Within this framework, to decrease the upper cell, one might turn to a decrease in wind-driven transport, an increase in eddy compensation, or both.

Since a wind-driven decrease in the upper cell of Southern Ocean during ice ages was first proposed, it has been explored and debated vigorously (Keeling & Visbeck, 2001; Sigman & Boyle, 2000; Toggweiler et al., 2006). There is not yet clear support from paleoclimate data (Kohfeld et al., 2013; Shulmeister et al., 2004) or models (Menviel et al., 2008; Rojas et al., 2009; Sime et al., 2013) for a weakening of the winds in the latitude range of the Drake Passage, which is most important for upwelling (Toggweiler et al., 2006). Even with a decline in northward Ekman transport, it has been argued that a parallel decline in the compensating transport by eddies will result in little change in the net upwelling and northward transport (Böning et al., 2008; Fischer et al., 2010; Keeling & Visbeck, 2001). However, there is also evidence that eddies do not fully

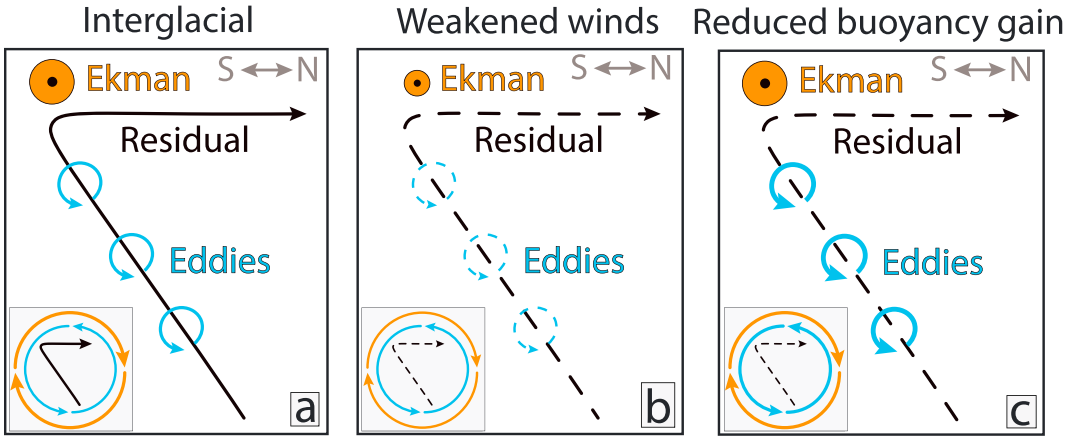

Figure 8. The Southern Ocean upper cell and two scenarios by which it might weaken during ice ages. In all cases, upwelling (black) reflects the wind-driven Ekman circulation (orange) less the countervailing eddy transport (blue). (a) Interglacial condition. (b) Reduced westerly wind stress on the Antarctic Zone surface may cause a decline in the magnitude of upwelling (Toggweiler et al., 2006), despite partial eddy compensation (Keeling & Visbeck, 2001). (c) A reduction in buoyancy gain by northward flowing Antarctic Zone surface water steepens isopycnals and increases eddy compensation without a corresponding rise in Ekman pumping, resulting in decreased residual upwelling (Watson & Naveira Garabato, 2006). Inset panels indicate the changing strengths of the opposing effects of the Southern Hemisphere westerly winds and eddies.

compensate for changes in surface wind stress (Figure 8b; Hallberg & Gnanadesikan, 2006). Moreover, there is some paleoceanographic evidence for a deglacial increase in the formation rate of Antarctic Intermediate Water, consistent with our interpretation of a weaker upper cell during ice ages (Pahnke & Zahn, 2005).

If there was a decline in northward Ekman transport as part of the upper cell, it likely would have been complemented by a decline in the rate of buoyancy gain by the northward flowing surface waters, simply because of the transport of less cold water to lower latitudes. If the wind-driven transport did not decline, then an independent decline in the gain of buoyancy (heat plus fresh water) by northward flowing surface waters could still have caused a slowing of the upper cell's residual circulation by enhancing the compensating eddy-driven flow (Figure 8c), as proposed by Watson and Naveira Garabato (2006). This reduced ocean heat uptake might have been caused by a focused cooling in the mid-latitudes (40°–55°S) during the last ice age. Indeed, an ice age reduction in net latent heat input (i.e., a reduction in precipitation minus evaporation) is expected for this region (Boos, 2012). However, enhancement of the compensating eddy-driven flow would have involved increased isopycnal exchange in the interior (Figure 8c), and this appears to lead to increased exchange between the surface mixed layer and the ocean interior (Abernathey & Ferreira, 2015), simplified as basal mixing in our model. Thus, it is possible that the mechanism of Watson and Naveira Garabato (2006) would not have decreased gross NO_3^- supply adequately to satisfy our model findings.

In summary, Toggweiler et al. (2006) and Watson and Naveira Garabato (2006) provide plausible physical mechanisms for an ice age slowing of the upper overturning cell in the Southern Ocean. Our finding that such a slowing did indeed occur calls for more exploration as to the ice age state of the Southern Hemisphere westerly winds as well as atmosphere/ocean buoyancy fluxes in the Southern Hemisphere mid-latitudes, two types of change that may well be related.

5. Concluding Remarks

Here we use a seasonally resolved two-layer model of the Antarctic Zone of the Southern Ocean to quantify the reduction of surface-deep exchange required to explain the coupled evidence of enhanced NO_3^- consumption and reduced export production during ice ages. Overall, we conclude that observations of a ~3‰–4‰ increase in diatom-bound $\delta^{15}N$ require an ice age reduction in the gross NO_3^- supply of >80%. This large decline implicates a weakening of the upper cell of the Southern Ocean overturning, most likely due to a reduction in Southern Hemisphere westerly wind-driven upwelling, as the initiator of the changes in the Antarctic upper ocean that contributed to reduced atmospheric CO_2 during ice ages.

Acknowledgments

P. C. K. was supported by the Fannie and John Hertz Foundation Susan & Richard Miles Graduate Fellowship and the Princeton Environmental Institute's Undergraduate Research Fund for senior thesis research. This research was conducted with government support under and awarded by DoD, Air Force Office of Scientific Research, National Defense Science and Engineering Graduate (NDSEG) Fellowship, 32 CFR 168a. The research was also supported by the National Science Foundation through grant PLR-1401489 (D. M. S.), by ExxonMobil through the Andlinger Center for Energy and the Environment at Princeton University, and by the Grand Challenges Program of Princeton University. M. P. H. acknowledges the NERC Independent Research Fellowship NE/K00901X/1, and S. E. F. acknowledges the South African National Research Foundation (grants 105895 and 105539). We are grateful to J. Adkins and R. Abernathey for insightful discussions regarding the residual circulation of the Southern Ocean, G. Viglione for sharing observations from the Southern Ocean, J. Rae for suggesting that we address possible changes in CDW [NO_3^-], R. Keeling and T. Trull for suggesting possible roles for mixed layer depth change, N. Klimovich for mathematical assistance, and A. Philips for advice on figure design. We also thank T. Trull and E. Sikes as well as anonymous reviewers for insightful reviews. The model described in this article is available as supporting material and can be used to generate the output reported here.

References

Abernathey, R., & Ferreira, D. (2015). Southern Ocean isopycnal mixing and ventilation changes driven by winds. *Geophysical Research Letters*, *42*, 10,357–10,365. https://doi.org/10.1002/2015GL066238

Abernathey, R. P., Cerovecki, I., Holland, P. R., Newsom, E., Mazloff, M., & Talley, L. D. (2016). Water-mass transformation by sea ice in the upper branch of the Southern Ocean overturning. *Nature Geoscience*, *9*(8), 596–601.

Altabet, M. A., Deuser, W. G., Honjo, S., & Stienen, C. (1991). Seasonal and depth-related changes in the source of sinking particles in the North Atlantic. *Nature*, *354*(6349), 136.

Altabet, M. A., & François, R. (1994). Sedimentary nitrogen isotopic ratio as a recorder for surface ocean nitrate utilization. *Global Biogeochemical Cycles*, *8*(1), 103–116. https://doi.org/10.1029/93GB03396

Altabet, M. A., & François, R. (2001). Nitrogen isotope biogeochemistry of the Antarctic polar frontal zone at 170°W. *Deep Sea Research Part II: Topical Studies in Oceanography*, *48*(19), 4247–4273.

Altabet, M. A., & Small, L. F. (1990). Nitrogen isotopic ratios in fecal pellets produced by marine zooplankton. *Geochimica et Cosmochimica Acta*, *54*(1), 155–163.

Anderson, R. F., Ali, S., Bradtmiller, L. I., Nielsen, S. H. H., Fleisher, M. Q., Anderson, B. E., & Burckle, L. H. (2009). Wind-driven upwelling in the Southern Ocean and the deglacial rise in atmospheric CO_2. *Science*, *323*(5920), 1443–1448.

Anderson, R. F., Chase, Z., Fleisher, M. Q., & Sachs, J. (2002). The Southern Ocean's biological pump during the last glacial maximum. *Deep Sea Research Part II: Topical Studies in Oceanography*, *49*(9–10), 1909–1938.

Berelson, W. M. (2001). The flux of particulate organic carbon into the ocean interior: A comparison of four US JGOFS regional studies. *Oceanography*, *14*(4), 59–67.

Bianchi, M., Feliatra, F., Tréguer, P., Vincendeau, M. A., & Morvan, J. (1997). Nitrification rates, ammonium and nitrate distribution in upper layers of the water column and in sediments of the Indian sector of the Southern Ocean. *Deep Sea Research Part II: Topical Studies in Oceanography*, *44*(5), 1017–1032.

Böning, C. W., Dispert, A., Visbeck, M., Rintoul, S. R., & Schwarzkopf, F. U. (2008). The response of the Antarctic circumpolar current to recent climate change. *Nature Geoscience*, *1*(12), 864.

Boos, W. R. (2012). Thermodynamic scaling of the hydrological cycle of the last glacial maximum. *Journal of Climate*, *25*(3), 992–1006.

Bouttes, N., Paillard, D., & Roche, D. M. V. A. P. (2010). Impact of brine-induced stratification on the glacial carbon cycle. *Climate of the Past*, *6*(5), 575–589.

Brunelle, B. G., Sigman, D. M., Cook, M. S., Keigwin, L. D., Haug, G. H., Plessen, B., Schettler, G., et al. (2007). Evidence from diatom-bound nitrogen isotopes for subarctic Pacific stratification during the last ice age and a link to North Pacific denitrification changes. *Paleoceanography*, *22*, PA1215. https://doi.org/10.1029/2005PA001205

Capone, D. G., Bronk, D. A., Mulholland, M. R., & Carpenter, E. J. (Eds.) (2008). *Nitrogen in the marine environment*. Burlington, MA: Academic Press.

Casciotti, K. L., Sigman, D. M., & Ward, B. B. (2003). Linking diversity and stable isotope fractionation in ammonia-oxidizing bacteria. *Geomicrobiology Journal*, *20*(4), 335–353.

Checkley, D. M., & Miller, C. A. (1989). Nitrogen isotope fractionation by oceanic zooplankton. *Deep Sea Research Part A. Oceanographic Research Papers*, *36*(10), 1449–1456.

Claquin, P., Martin-Jézéquel, V., Kromkamp, J. C., Veldhuis, M. J., & Kraay, G. W. (2002). Uncoupling of silicon compared with carbon and nitrogen metabolisms and the role of the cell cycle in continuous cultures of *Thalassiosira pseudonana* (bacillariophyceae) under light, nitrogen, and phosphorus control. *Journal of Phycology*, *38*(5), 922–930.

Close, H. G., Shah, S. R., Ingalls, A. E., Diefendorf, A. F., Brodie, E. L., Hansman, R. L., Freeman, K. H., et al. (2013). Export of submicron particulate organic matter to mesopelagic depth in an oligotrophic gyre. *Proceedings of the National Academy of Sciences of the United States of America*, *110*(31), 12565–12570. https://doi.org/10.1073/pnas.1217514110

De Boer, A. M., & Hogg, A. M. (2014). Control of the glacial carbon budget by topographically induced mixing. *Geophysical Research Letters*, *41*, 4277–4284. https://doi.org/10.1002/2014GL059963

De Boer, A. M., Sigman, D. M., Toggweiler, J. R., & Russell, J. L. (2007). Effect of global ocean temperature change on deep ocean ventilation. *Paleoceanography*, *22*, PA2210. https://doi.org/10.1029/2005PA001242

De Boer, A. M., Toggweiler, J. R., & Sigman, D. M. (2008). Atlantic dominance of the meridional overturning circulation. *Journal of Physical Oceanography*, *38*(2), 435–450.

DeNiro, M. J., & Epstein, S. (1981). Influence of diet on the distribution of nitrogen isotopes in animals. *Geochimica et Cosmochimica Acta*, *45*(3), 341–351.

Deutsch, C., Sigman, D. M., Thunell, R. C., Meckler, A. N., & Haug, G. H. (2004). Isotopic constraints on glacial/interglacial changes in the oceanic nitrogen budget. *Global Biogeochemical Cycles*, *18*, GB4012. https://doi.org/10.1029/2003GB002189

DiFiore, P. J., Sigman, D. M., & Dunbar, R. B. (2009). Upper ocean nitrogen fluxes in the Polar Antarctic Zone: Constraints from the nitrogen and oxygen isotopes of nitrate. *Geochemistry, Geophysics, Geosystems*, *10*, Q11016. https://doi.org/10.1029/2009GC002468

DiFiore, P. J., Sigman, D. M., Karsh, K. L., Trull, T. W., Dunbar, R. B., & Robinson, R. S. (2010). Poleward decrease in the isotope effect of nitrate assimilation across the Southern Ocean. *Geophysical Research Letters*, *37*, L17601. https://doi.org/10.1029/2010GL044090

Dong, S., Sprintall, J., Gille, S. T., & Talley, L. (2008). Southern Ocean mixed-layer depth from Argo float profiles. *Journal of Geophysical Research*, *113*, C06013. https://doi.org/10.1029/2006JC004051

Fawcett, S. E., Lomas, M. W., Casey, J. R., Ward, B. B., & Sigman, D. M. (2011). Assimilation of upwelled nitrate by small eukaryotes in the Sargasso Sea. *Nature Geoscience*, *4*(10), 717–722.

Ferrari, R., Jansen, M. F., Adkins, J. F., Burke, A., Stewart, A. L., & Thompson, A. F. (2014). Antarctic sea ice control on ocean circulation in present and glacial climates. *Proceedings of the National Academy of Sciences of the United States of America*, *111*(24), 8753–8758.

Fischer, H., Schmitt, J., Lüthi, D., Stocker, T. F., Tschumi, T., Parekh, P., Joos, F., et al. (2010). The role of Southern Ocean processes in orbital and millennial CO_2 variations—A synthesis. *Quaternary Science Reviews*, *29*(1–2), 193–205. https://doi.org/10.1016/j.quascirev.2009.06.007

François, R., Altabet, M. A., Yu, E.-F., Sigman, D. M., Bacon, M. P., Frank, M., Bohrmann, G., et al. (1997). Contribution of Southern Ocean surface-water stratification to low atmospheric CO_2 concentrations during the last glacial period. *Nature*, *389*(6654), 929–935. https://doi.org/10.1038/40073

Fripiat, F., Sigman, D. M., Fawcett, S. E., Rafter, P. A., Weigand, M. A., & Tison, J. L. (2014). New insights into sea ice nitrogen biogeochemical dynamics from the nitrogen isotopes. *Global Biogeochemical Cycles*, *28*, 115–130. https://doi.org/10.1002/2013GB004729

Fry, B. (1988). Food web structure on Georges Bank from stable C, N, and S isotopic compositions. *Limnology and Oceanography*, *33*(5), 1182–1190.

Glibert, P. M., Biggs, D. C., & McCarthy, J. J. (1982). Utilization of ammonium and nitrate during austral summer in the Scotia Sea. *Deep Sea Research Part A. Oceanographic Research Papers*, *29*(7), 837–850.

Hain, M. P., Sigman, D. M., & Haug, G. H. (2010). Carbon dioxide effects of Antarctic stratification, North Atlantic Intermediate Water formation, and subantarctic nutrient drawdown during the last ice age: Diagnosis and synthesis in a geochemical box model. *Global Biogeochemical Cycles*, *24*, GB4023. https://doi.org/10.1029/2010GB003790

Hallberg, R., & Gnanadesikan, A. (2006). The role of eddies in determining the structure and response of the wind-driven Southern Hemisphere overturning: Results from the Modeling Eddies in the Southern Ocean (MESO) project. *Journal of Physical Oceanography*, *36*(12), 2232–2252.

Hayes, J. M. (2004). *An introduction to isotopic calculations* (p. 2543). Woods Hole, MA: Woods Hole Oceanographic Institution.

Horn, M. G., Robinson, R. S., Rynearson, T. A., & Sigman, D. M. (2011). Nitrogen isotopic relationship between diatom-bound and bulk organic matter of cultured polar diatoms. *Paleoceanography*, *26*, PA3208. https://doi.org/10.1029/2010PA002080

Houlton, B. Z., Sigman, D. M., & Hedin, L. O. (2006). Isotopic evidence for large gaseous nitrogen losses from tropical rainforests. *Proceedings of the National Academy of Sciences of the United States of America*, *103*(23), 8745–8750.

Hutchins, D. A., & Bruland, K. W. (1998). Iron-limited diatom growth and Si: N uptake ratios in a coastal upwelling regime. *Nature*, *393*(6685), 561.

Ito, T., & Follows, M. J. (2005). Preformed phosphate, soft tissue pump and atmospheric CO_2. *Journal of Marine Research*, *63*(4), 813–839.

Jaccard, S. L., Hayes, C. T., Martínez-García, A., Hodell, D. A., Anderson, R. F., Sigman, D. M., & Haug, G. H. (2013). Two modes of change in Southern Ocean productivity over the past million years. *Science*, *339*(6126), 1419–1423.

Jouzel, J., Masson-Delmotte, V., Cattani, O., Dreyfus, G., Falourd, S., Hoffmann, G., et al. (2007). Orbital and millennial Antarctic climate variability over the past 800,000 years. *Science*, *317*(5839), 793–796. https://doi.org/10.1126/science.1141038

Karsten, R. H., & Marshall, J. (2002). Constructing the residual circulation of the ACC from observations. *Journal of Physical Oceanography*, *32*(12), 3315–3327.

Keeling, R., & Visbeck, M. (2001). Palaeoceanography—Antarctic stratification and glacial CO_2. *Nature*, *412*, 605–606.

Kemeny, P. C., Weigand, M. A., Zhang, R., Carter, B. R., Karsh, K. L., Fawcett, S. E., & Sigman, D. M. (2016). Enzyme-level interconversion of nitrate and nitrite in the fall mixed layer of the Antarctic Ocean. *Global Biogeochemical Cycles*, *30*, 1069–1085. https://doi.org/10.1002/2015GB005350

Knox, F., & McElroy, M. B. (1984). Changes in atmospheric CO_2: Influence of the marine biota at high latitude. *Journal of Geophysical Research*, *89*, 4629–4637. https://doi.org/10.1029/JD089iD03p04629

Kohfeld, K. E., Graham, R. M., De Boer, A. M., Sime, L. C., Wolff, E. W., Le Quéré, C., & Bopp, L. (2013). Southern Hemisphere westerly wind changes during the Last Glacial Maximum: paleo-data synthesis. *Quaternary Science Reviews*, *68*, 76–95.

Kohfeld, K. E., Le Quéré, C., Harrison, S. P., & Anderson, R. F. (2005). Role of marine biology in glacial-interglacial CO_2 cycles. *Science*, *308*(5718), 74–78.

Koike, I., Holm-Hansen, O., & Biggs, D. C. (1986). Inorganic nitrogen metabolism by Antarctic phytoplankton with special reference to ammonium cycling. *Marine Ecology Progress Series*, *30*(2–3), 105–116.

Kumar, N., Anderson, R. F., Mortlock, R. A., Froelich, P. N., Kubik, P., Dittrich-Hannen, B., & Suter, M. (1995). Increased biological productivity and export production in the glacial Southern Ocean. *Nature*, *378*(6558), 675.

Kumar, N., Gwiazda, R., Anderson, R. F., & Froelich, P. N. (1993). $^{231}Pa/^{230}Th$ ratios in sediments as a proxy for past changes in Southern Ocean productivity. *Nature*, *362*(6415), 45.

Lefèvre, N., & Watson, A. J. (1999). Modeling the geochemical cycle of iron in the oceans and its impact on atmospheric CO_2 concentrations. *Global Biogeochemical Cycles*, *13*(3), 727–736. https://doi.org/10.1029/1999GB900034

Lourey, M. J., Trull, T. W., & Sigman, D. M. (2003). Sensitivity of $\delta^{15}N$ of nitrate, surface suspended and deep sinking particulate nitrogen to seasonal nitrate depletion in the Southern Ocean. *Global Biogeochemical Cycles*, *17*(3), 1081. https://doi.org/10.1029/2002GB001973

Lund, D. C., Adkins, J. F., & Ferrari, R. (2011). Abyssal Atlantic circulation during the Last Glacial Maximum: Constraining the ratio between transport and vertical mixing. *Paleoceanography*, *26*, PA1213. https://doi.org/10.1029/2010PA001938

Marshall, D. (1997). Subduction of water masses in an eddying ocean. *Journal of Marine Research*, *55*(2), 201–222.

Marshall, J., & Radko, T. (2003). Residual-mean solutions for the Antarctic Circumpolar Current and its associated overturning circulation. *Journal of Physical Oceanography*, *33*(11), 2341–2354.

Marshall, J., & Radko, T. (2006). A model of the upper branch of the meridional overturning of the southern ocean. *Progress in Oceanography*, *70*(2), 331–345.

Marshall, J., Shuckburgh, E., Jones, H., & Hill, C. (2006). Estimates and implications of surface eddy diffusivity in the Southern Ocean derived from tracer transport. *Journal of Physical Oceanography*, *36*(9), 1806–1821.

Marshall, J., & Speer, K. (2012). Closure of the meridional overturning circulation through Southern Ocean upwelling. *Nature Geoscience*, *5*(3), 171–180.

Martin, J. H. (1990). Glacial-interglacial CO_2 change: The iron hypothesis. *Paleoceanography*, *5*(1), 1–13. https://doi.org/10.1029/PA005i001p00001

Martin, J. H., Knauer, G. A., Karl, D. M., & Broenkow, W. W. (1987). VERTEX: Carbon cycling in the northeast Pacific. *Deep Sea Research Part A. Oceanographic Research Papers*, *34*(2), 267–285.

Martínez-García, A., Sigman, D. M., Ren, H., Anderson, R. F., Straub, M., Hodell, D. A., et al. (2014). Iron fertilization of the Subantarctic Ocean during the last ice age. *Science*, *343*(6177), 1347–1350.

Martiny, A. C., Vrugt, J. A., Primeau, F. W., & Lomas, M. W. (2013). Regional variation in the particulate organic carbon to nitrogen ratio in the surface ocean. *Global Biogeochemical Cycles*, *27*, 723–731. https://doi.org/10.1002/gbc.20061

Menviel, L., Timmermann, A., Mouchet, A., & Timm, O. (2008). Climate and marine carbon cycle response to changes in the strength of the Southern Hemispheric westerlies. *Paleoceanography*, *23*, PA4201. https://doi.org/10.1029/2008PA001604

Michaels, A. F., & Silver, M. W. (1988). Primary production, sinking fluxes and the microbial food web. *Deep Sea Research Part A. Oceanographic Research Papers*, *35*(4), 473–490.

Minagawa, M., & Wada, E. (1984). Stepwise enrichment of ^{15}N along food chains: Further evidence and the relation between $\delta^{15}N$ and animal age. *Geochimica et Cosmochimica Acta*, *48*(5), 1135–1140.

Mitchell, B. G., Brody, E. A., Holm-Hansen, O., McClain, C., & Bishop, J. (1991). Light limitation of phytoplankton biomass and macronutrient utilization in the Southern Ocean. *Limnology and Oceanography*, *36*(8), 1662–1677.

Morales, L. V., Granger, J., Chang, B. X., Prokopenko, M. G., Plessen, B., Gradinger, R., & Sigman, D. M. (2014). Elevated $^{15}N/^{14}N$ in particulate organic matter, zooplankton, and diatom frustule-bound nitrogen in the ice-covered water column of the Bering Sea eastern shelf. *Deep Sea Research Part II: Topical Studies in Oceanography*, *109*, 100–111.

Morales, L. V., Sigman, D. M., Horn, M. G., & Robinson, R. S. (2013). Cleaning methods for the isotopic determination of diatom-bound nitrogen in non-fossil diatom frustules. *Limnology and Oceanography: Methods*, *11*(2), 101–112.

Mortlock, R. A., Charles, C. D., Froelich, P. N., Zibello, M. A., Saltzman, J., Hays, J. D., & Burckle, L. H. (1991). Evidence for lower productivity in the Antarctic Ocean during the last glaciation. *Nature*, *351*(6323), 220–223.

Munro, D. R., Lovenduski, N. S., Stephens, B. B., Newberger, T., Arrigo, K. R., Takahashi, T., et al. (2015). Estimates of net community production in the Southern Ocean determined from time series observations (2002–2011) of nutrients, dissolved inorganic carbon, and surface ocean pCO_2 in Drake Passage. *Deep Sea Research Part II: Topical Studies in Oceanography*, *114*, 49–63. https://doi.org/10.1016/j.dsr2.2014.12.014

Olson, R. J. (1980). Nitrate and ammonium uptake in Antarctic waters. *Limnology and Oceanography*, *25*(6), 1064–1074.

Orsi, A. H., Whitworth, T., & Nowlin, W. D. (1995). On the meridional extent and fronts of the Antarctic Circumpolar Current. *Deep Sea Research Part I: Oceanographic Research Papers*, *42*(5), 641–673.

Pahnke, K., & Zahn, R. (2005). Southern Hemisphere water mass conversion linked with North Atlantic climate variability. *Science*, *307*(5716), 1741–1746.

Rafter, P. A., Sigman, D. M., & Mackey, K. R. (2017). Recycled iron fuels new production in the eastern equatorial Pacific Ocean. *Nature Communications*, *8*, 1100.

Rau, G. H., Sullivan, C. W., & Gordon, L. I. (1991). $\delta^{13}C$ and $\delta^{15}N$ variations in Weddell Sea particulate organic matter. *Marine Chemistry*, *35*(1–4), 355–369.

Robinson, R. S., Brunelle, B. G., & Sigman, D. M. (2004). Revisiting nutrient utilization in the glacial Antarctic: Evidence from a new method for diatom-bound N isotopic analysis. *Paleoceanography*, *19*, PA3001. https://doi.org/10.1029/2003PA000996

Robinson, R. S., & Sigman, D. M. (2008). Nitrogen isotopic evidence for a poleward decrease in surface nitrate within the ice age Antarctic. *Quaternary Science Reviews*, *27*(9), 1076–1090.

Rojas, M., Moreno, P., Kageyama, M., Crucifix, M., Hewitt, C., Abe-Ouchi, A., et al. (2009). The southern westerlies during the last glacial maximum in PMIP2 simulations. *Climate Dynamics*, *32*(4), 525–548. https://doi.org/10.1007/s00382-008-0421-7

Rönner, U., Sörensson, F., & Holm-Hansen, O. (1983). Nitrogen assimilation by phytoplankton in the Scotia Sea. *Polar Biology*, *2*(3), 137–147.

Rubin, S. I., Takahashi, T., Chipman, D. W., & Goddard, J. G. (1998). Primary productivity and nutrient utilization ratios in the Pacific sector of the Southern Ocean based on seasonal changes in seawater chemistry. *Deep Sea Research Part I: Oceanographic Research Papers*, *45*(8), 1211–1234.

Sallée, J. B., Speer, K., Rintoul, S., & Wijffels, S. (2010). Southern Ocean thermocline ventilation. *Journal of Physical Oceanography*, *40*(3), 509–529.

Sambrotto, R. N., & Mace, B. J. (2000). Coupling of biological and physical regimes across the Antarctic Polar Front as reflected by nitrogen production and recycling. *Deep Sea Research Part II: Topical Studies in Oceanography*, *47*(15–16), 3339–3367.

Sarmiento, J. L., & Toggweiler, J. R. (1984). A new model for the role of the oceans in determining atmospheric pCO_2. *Nature*, *308*(5960), 621–624.

Sarthou, G., Timmermans, K. R., Blain, S., & Tréguer, P. (2005). Growth physiology and fate of diatoms in the ocean: A review. *Journal of Sea Research*, *53*(1–2), 25–42.

Sharma, G. S., & Mathew, B. (1985). Hydrography and circulation off the Antarctica in the Indian Ocean region. *Proceedings of the Indian Academy of Sciences-Earth and Planetary Sciences*, *94*(1), 13–27.

Shulmeister, J., Goodwin, I., Renwick, J., Harle, K., Armand, L., McGlone, M. S., et al. (2004). The Southern Hemisphere westerlies in the Australasian sector over the last glacial cycle: A synthesis. *Quaternary International*, *118*, 23–53.

Siegenthaler, U., & Wenk, T. (1984). Rapid atmospheric CO_2. *Nature*, *308*, 12.

Sigman, D. M., Altabet, M. A., François, R., McCorkle, D. C., & Gaillard, J. F. (1999). The isotopic composition of diatom-bound nitrogen in Southern Ocean sediments. *Paleoceanography*, *14*(2), 118–134. https://doi.org/10.1029/1998PA900018

Sigman, D. M., & Boyle, E. A. (2000). Glacial/interglacial variations in atmospheric carbon dioxide. *Nature*, *407*(6806), 859–869.

Sigman, D. M., Hain, M. P., & Haug, G. H. (2010). The polar ocean and glacial cycles in atmospheric CO_2 concentration. *Nature*, *466*(7302), 47–55.

Sigman, D. M., Jaccard, S. L., & Haug, G. H. (2004). Polar ocean stratification in a cold climate. *Nature*, *428*(6978), 59–63.

Sime, L. C., Kohfeld, K. E., Le Quéré, C., Wolff, E. W., de Boer, A. M., Graham, R. M., & Bopp, L. (2013). Southern Hemisphere westerly wind changes during the Last Glacial Maximum: Model-data comparison. *Quaternary Science Reviews*, *64*, 104–120.

Smart, S. M., Fawcett, S. E., Thomalla, S. J., Weigand, M. A., Reason, C. J., & Sigman, D. M. (2015). Isotopic evidence for nitrification in the Antarctic winter mixed layer. *Global Biogeochemical Cycles*, *29*, 427–445. https://doi.org/10.1002/2014GB005013

Smetacek, V., & Passow, U. (1990). Spring bloom initiation and Sverdrup's critical-depth model. *Limnology and Oceanography*, *35*(1), 228–234.

Studer, A. S., Sigman, D. M., Martínez-García, A., Benz, V., Winckler, G., Kuhn, G., et al. (2015). Antarctic zone nutrient conditions during the last two glacial cycles. *Paleoceanography*, *30*, 845–862. https://doi.org/10.1002/2014PA002745

Sunda, W. G., & Huntsman, S. A. (1997). Interrelated influence of iron, light and cell size on marine phytoplankton growth. *Nature*, *390*(6658), 389–392.

Sweeney, C., Smith, W. O., Hales, B., Bidigare, R. R., Carlson, C. A., Codispoti, L. A., et al. (2000). Nutrient and carbon removal ratios and fluxes in the Ross Sea, Antarctica. *Deep Sea Research Part II: Topical Studies in Oceanography*, *47*(15-16), 3395–3421. https://doi.org/10.1016/S0967-0645(00)00073-4

Tagliabue, A., Sallée, J. B., Bowie, A. R., Lévy, M., Swart, S., & Boyd, P. W. (2014). Surface-water iron supplies in the Southern Ocean sustained by deep winter mixing. *Nature Geoscience*, *7*(4), 314–320.

Takeda, S. (1998). Influence of iron availability on nutrient consumption ratio of diatoms in oceanic waters. *Nature*, *393*(6687), 774.

Thunell, R. C., Sigman, D. M., Muller-Karger, F., Astor, Y., & Varela, R. (2004). Nitrogen isotope dynamics of the Cariaco Basin, Venezuela. *Global Biogeochemical Cycles*, *18*, GB3001. https://doi.org/10.1029/2003GB002185

Toggweiler, J. R., Russell, J. L., & Carson, S. R. (2006). Midlatitude westerlies, atmospheric CO_2, and climate change during the ice ages. *Paleoceanography*, *21*, PA2005. https://doi.org/10.1029/2005PA001154

Trull, T. W., Davies, D. M., Dehairs, F., Cavagna, A. J., Lasbleiz, M., Laurenceau-Cornec, E. C., et al. (2015). Chemometric perspectives on plankton community responses to natural iron fertilisation over and downstream of the Kerguelen plateau in the Southern Ocean. *Biogeosciences*, *12*(4), 1029–1056. https://doi.org/10.5194/bg-12-1029-2015

Vo, J., Inwood, W., Hayes, J. M., & Kustu, S. (2013). Mechanism for nitrogen isotope fractionation during ammonium assimilation by Escherichia coli K12. *Proceedings of the National Academy of Sciences of the United States of America*, *110*(21), 8696–8701.

Wada, E., Terazaki, M., Kabaya, Y., & Nemoto, T. (1987). ^{15}N and ^{13}C abundances in the Antarctic Ocean with emphasis on the biogeochemical structure of the food web. *Deep Sea Research Part A. Oceanographic Research Papers*, *34*(5–6), 829–841.

Waite, A. M., Safi, K. A., Hall, J. A., & Nodder, S. D. (2000). Mass sedimentation of picoplankton embedded in organic aggregates. *Limnology and Oceanography*, *45*(1), 87–97.

Watson, A. J., & Naveira Garabato, A. C. (2006). The role of Southern Ocean mixing and upwelling in glacial-interglacial atmospheric CO_2 change. *Tellus B*, *58*(1), 73–87.

Watson, A. J., Vallis, G. K., & Nikurashin, M. (2015). Southern Ocean buoyancy forcing of ocean ventilation and glacial atmospheric CO_2. *Nature Geoscience*, *8*(11), 861–864.

Weber, T., Cram, J. A., Leung, S. W., DeVries, T., & Deutsch, C. (2016). Deep ocean nutrients imply large latitudinal variation in particle transfer efficiency. *Proceedings of the National Academy of Sciences of the United States of America*, *113*(31), 8606–8611.